NACA

RESEARCH MEMORANDUM

A FLIGHT INVESTIGATION AT TRANSONIC SPEEDS OF A MODEL HAVING A TRIANGULAR WING OF ASPECT RATIO 2

By Maurice D. White

Ames Aeronautical Laboratory
Moffett Field, Calif.

NATIONAL ADVISORY COMMITTEE
FOR AERONAUTICS

WASHINGTON

September 7, 1955

NATIONAL ADVISORY COMMITTEE FOR AERONAUTICS

RESEARCH MEMORANDUM

A FLIGHT INVESTIGATION AT TRANSONIC SPEEDS OF A MODEL HAVING A TRIANGULAR WING OF ASPECT RATIO 2

By Maurice D. White

SUMMARY

Free-falling recoverable model tests were conducted at transonic speeds on a model having a triangular wing of aspect ratio 2 and a 45° swept tail located in the chord plane of the wing. Static- and dynamic-longitudinal-stability data for the complete model, force and moment data for the major components of the model, and load distributions over the fuselage of the model were evaluated at angles of attack up to about 25° to 30° depending on the Mach number.

The results of these tests indicated that at small angles of attack large variations of downwash angle with angle of attack occurred at the test tail location, similar to those reported in other tests of low-aspect-ratio wings having tails located in the wing-chord plane. The drag-rise-with-lift factor for the wing was found to decrease generally with increasing Mach number, or perhaps more significantly, with simultaneously increasing Reynolds number through the transonic Mach number range covered by the tests. The dominant influence of Reynolds number was further suggested by a similarity noted between the variations with Reynolds number of the drag-rise-with-lift factor for a family of triangular wings and the variations with Reynolds number of the pressure distribution over swept circular cylinders. The experimental increase in minimum drag for the complete model through the transonic Mach number range was closely predicted by use of available methods.

INTRODUCTION

As part of a general investigation of the characteristics of low-aspect-ratio wings, flight tests were conducted on a model having a triangular wing of aspect ratio 2 with an NACA 0005-63 airfoil section and a 45° swept horizontal tail. The flight tests of the same fuselage-tail combination with other wings were reported in references 1, 2, 3, and 4. The wings reported on in references 3 and 4 differ from that reported on here

only in aspect ratio. Wings of the same plan form as the present flight-test wing, but not necessarily the same airfoil section, have been tested in other facilities (see, e.g., refs. 5 and 6).

In the present investigation the range of previous wind-tunnel investigations was extended in the following particulars:

1. High Reynolds numbers (11 million to 25 million) were covered at transonic Mach numbers (0.8 to 1.1).

2. Dynamic- as well as static-longitudinal-stability characteristics of the model were obtained.

3. Loading distributions over the fuselage of the model were obtained.

4. Aerodynamic forces and moments were evaluated for the complete model as well as for the major components of the model, the wing, the fuselage, and, by taking differences, the tail.

The tests were made by the Ames Aeronautical Laboratory using the free-falling recoverable-model technique in an area provided by the Air Force at Edwards Air Force Base, Edwards, California.

SYMBOLS

A	aspect ratio
b	wing span, ft
c	local chord, ft
$\bar{c}$	mean aerodynamic chord of the wing, $\frac{2}{S}\int_0^{b/2} c^2 dy$, ft
I_y	moment of inertia of the model about the Y axis, slug-ft^2
M	Mach number
p	static pressure, lb/sq ft
p_c	pressure on the surface of a cylinder, lb/sq ft
p_o	ambient pressure, lb/sq ft
P	pressure coefficient on the surface of a cylinder, $\frac{p_c - p_o}{q_o}$

ΔP $\quad \dfrac{p_l - p_u}{q_o}$

q angular velocity in pitch, radians/sec

q_o dynamic pressure, lb/sq ft

$\dot{q}$ angular acceleration in pitch, radians/sec^2

R Reynolds number based on $\bar{c}$

r radius of fuselage at longitudinal station x, in.

S wing area, including the area formed by extending the leading and trailing edges to the plane of symmetry, sq ft

V speed, ft/sec

x longitudinal distance from fuselage station 0, in.

y spanwise distance from model center line, ft

C_D drag coefficient, $\dfrac{\text{drag}}{q_o S}$

C_L lift coefficient, $\dfrac{\text{lift}}{q_o S}$

C_m pitching-moment coefficient,

$$\frac{\text{pitching moment about center of gravity}}{q_o S \bar{c}}$$

C_{m_q} $\quad \dfrac{\partial C_m}{\partial (q\bar{c}/2V)}$

$C_{m_{\dot{\alpha}}}$ $\quad \dfrac{\partial C_m}{\partial (\dot{\alpha}\bar{c}/2V)}$

α angle of attack, deg

$\dot{\alpha}$ rate of change at angle of attack, radians/sec

δ deflection of horizontal tail, deg

ϵ downwash angle, deg

Subscripts

l	lower surface of the fuselage
u	upper surface of the fuselage
max	maximum
min	minimum
α,δ	derivative of the factor with respect to the subscript, as $C_{L_\alpha} = \frac{\partial C_L}{\partial \alpha}$, etc.

MODEL

A three-view drawing of the complete model is shown in figure 1 and pertinent dimensions are listed in table I. A photograph of the model, taken immediately after release from the carrier airplane, is shown in figure 2. Shown attached to the model in figure 2 is the jettisonable booster which was used in some of the drops to obtain higher Mach numbers.

The wing was of triangular plan form with an aspect ratio of 2. The airfoil section was the NACA 0005-63 parallel to the free stream; ordinates of this airfoil section are listed in table II. The wing panels were constructed with a steel core and a wood covering, the whole covered with plastic impregnated glass cloth, and were mounted so as to permit measurement of the forces on the exposed portions. The juncture of the wing root and the fuselage was sealed with a flexible rubber seal.

All other components of the model were as described in reference 7.

INSTRUMENTATION

Forces and moments on the exposed wing panels were measured on an internal strain-gage balance. Forces and moments on the complete model were determined by accelerometer measurements. The instrumentation was identical to that described in reference 1 except that potentiometers were substituted for selsyns as transducers for the angle-of-attack and the angle-of-sideslip vanes shown in figure 1.

TESTS

The test procedure used was the same as that described in reference 7; that is, the model was released from the carrier airplane at high altitude and allowed to accelerate in free fall. After the test Mach number was attained, the horizontal control was pulsed intermittently, and data were recorded during the ensuing control-fixed oscillations. At the conclusion of the tests the model was decelerated by opening a dive brake, and was finally eased to the ground on a parachute. For some drops, rocket assist was employed in order to increase the attainable Mach number. The booster rocket (fig. 2) was jettisoned at the conclusion of boost and prior to the actual test period.

The Mach numbers of the tests ranged from about 0.8 to 1.1, the Reynolds numbers from 11 million to 25 million (fig. 3), and the angles of attack from -2° to 30° for Mach numbers less than about 0.95, and from -1° to 25° for Mach numbers greater than 0.95. The center of gravity was moved from $0.397\bar{c}$ for some drops to $0.467\bar{c}$ for other drops in order to attain higher angles of attack with the available control.

Data are presented in this report for five settings of the horizontal tail. Each horizontal-tail angle is identified with a different trim angle-of-attack curve in figure 4.

PRECISION OF MEASUREMENT

Based upon instrument precisions and their effect on the computed coefficients, the estimated incremental error of any one reading is believed to be within the values listed below:

Item	Estimated maximum error	
	M = 0.85	M = 1.05
Mach number	±0.01	±0.01
Angle of attack	$\pm 1/4^\circ$	$\pm 1/4^\circ$
C_L (complete model)	±0.02	±0.009
C_L (wing)	±0.02	±0.008
C_D (complete model)	±.002	±.001
C_D (wing)	±.006	±.002
C_m (complete model)	±.001	±.001
$C_{m_{\bar{c}/4}}$ (wing)	±.004	±.002

The over-all accuracy of the final results is, of course, a function of factors additional to the precision of the instruments, but to which it is difficult to assign quantitative values. For example, the accuracy of

any one "static" data point is reduced by the fact that it is determined through time correlation of a number of rapidly varying records. However, in deriving the curves showing the variation of a "static" quantity with, say, angle of attack, a large number of data points is considered, which helps to define more closely the correct fairing of the data. Also, shifts in the data which occurred from drop to drop were usually definable to a close degree by reference to a number of different records, and by the fact that the entire configuration was symmetrical with control undeflected. Consideration of all these factors leads to the conclusion that the accuracy of "static" results which were obtained by fairing the flight data is of the order of the values listed above.

RESULTS

In general, the flight data were evaluated by the methods described in reference 7. The results are identified as applying to the following:

1. The exposed wing panel.

2. The total wing, obtained by adding to the data for the exposed wing panels, the data obtained by integrating the pressure differences over the fuselage over the area where they were measured, stations 40 to 135.5. An additional total-wing drag increment was obtained by applying a skin-friction coefficient of 0.0028 to the entire fuselage surface area between stations 40 and 135.5.

3. The complete model.

Lift

In figure 5 curves are presented of C_L against α for the test Mach number range, and in figure 6 the lift-curve slopes for the various components are plotted as a function of Mach number. In presenting the lift-curve slopes for the complete model in figure 6, it was assumed that the slopes were unaffected by deflections of the horizontal tail and accordingly no corrections were made for this factor.

Drag

Curves of C_D against C_L for the various components are plotted in figure 7 for various Mach numbers. In figures 8 and 9 are plotted,

respectively, as a function of Mach number, the values of $C_{D_{min}}$ for the total wing and the complete model, and the values of the drag-rise factor $\partial C_D/\partial C_L^2$ for the exposed wing, the total wing, and the complete model. Except at the lowest test Mach numbers, the curves of C_D against C_L^2 from which the latter values were obtained were reasonably linear up to a value of C_L of about 0.25.

Static Longitudinal Stability

The variation of trim angle of attack with Mach number for several horizontal-tail positions is shown in figure 4.

In figure 10(a) are shown the variation with angle of attack of C_m for the complete model as determined from $C_m = I_y\dot{q}/q_oS\bar{c}$, by use of the data-evaluation procedures described in reference 7. A slight departure from the method of reference 7 was made in that the small effects of pitch damping were eliminated by fairing between positive and negative pitching velocities rather than by calculating the magnitudes of the damping contribution from the equation. Also shown in figure 10(a) are straight lines having the slope C_{m_α} as determined from the periods of the control-fixed oscillations. For clarity of presentation these lines are drawn displaced in C_m from their actual locations by arbitrary amounts. No lines for C_{m_α} are shown for the drop defined in figure 4 by $\delta = -16^\circ$, because the oscillations were not regular enough to give a well-defined period in the presence of the stalling that occurred in that drop.

Curves of C_m against α for the complete model have been calculated for $\delta = 0^\circ$ for a center-of-gravity location of 0.25c for the complete angle-of-attack range covered by the tests, by applying corrections to the data of figure 10(a) for differences in center-of-gravity location and in horizontal-tail setting. The calculated curves are presented in figure 10(b) together with corresponding curves for the exposed wing panels and the total wing. The pitching-moment coefficients contributed by the tail with $\delta = 0^\circ$, as determined by subtracting from the complete model data the data for the total wing, are also included in figure 10(b). By this method of evaluation the value of C_m contributed by the tail will include the contribution of the portion of the fuselage where pressures were not measured. The magnitude of this contribution is believed to be inconsequential in relation to that of the tail.

The wing pitching moments about the wing quarter-chord point have been plotted in figure 11 in terms of C_m against C_L. The variations with Mach number of the aerodynamic-center location for the total wing and for the complete model at small angles of attack are shown in figure 12.

Dynamic Longitudinal Stability

Values of $C_{m_q} + C_{m_{\dot{\alpha}}}$ for the complete model are shown in figure 13 as a function of Mach number. These values were obtained in the usual manner as described in reference 8; that is, by deducting the contribution of the lift-curve slope from the total damping factor that was obtained from analysis of the control-fixed oscillations of the model.

Horizontal-Tail Effectiveness

The variation with Mach number of the horizontal-tail-effectiveness parameter C_{m_δ} is shown in figure 14. Two methods were used to evaluate this parameter. One method was to plot C_m for the complete model against δ during a control pulse, selecting data only for regimes where α was reasonably constant. The second method used was to plot as a function of $\Delta\delta_{trim}$ the change in C_m for the complete model that would be required to aline the curves of figure 10 for $\delta \neq 0^\circ$ with those for $\delta = 0^\circ$.

Loading Distribution Over Fuselage

In figure 15 are plotted the distributions of loading along the fuselage center line and along a line displaced circumferentially 45° from the center line. The locations of the orifices from which the data were obtained are shown in figure 16. The data represent the difference in pressure coefficient between corresponding orifices on the top and bottom of the fuselage.

DISCUSSION

Lift

The lift curves of figure 5 show considerable nonlinearity in certain regions. At small angles of attack, particularly at Mach numbers in the vicinity of 0.92, the data for the wing show an increasing lift-curve slope with increasing angle of attack. At higher angles of attack, for all Mach numbers, the lift-curve slope decreases with increasing angle of attack. These nonlinearities are also evidenced by data from the Ames 12-foot and 6- by 6-foot wind tunnels (ref. 5), and the Ames 16-foot wind tunnel bump (ref. 6), shown for comparison in figure 17. The probable source of the nonlinearities at small angles of attack is discussed in reference 9 in which it is shown that separation of the flow at the leading edge of the wing would account for the observed effects. The fact that the nonlinearities at small angles of attack tend to disappear at the higher Mach

numbers (and correspondingly higher Reynolds numbers) of these tests may indicate that the critical Reynolds number for leading-edge separation was exceeded. Additional evidence of this effect is discussed in the following section on drag.

The lift curves for the complete model with the horizontal tail undeflected are virtually the same as those for the total wing at small angles of attack. The range of angles of attack for which the data coincided was greatest for Mach numbers above 0.96. Generally, as the angle of attack was increased, the slope of the lift curve for the complete model increased more than did the slope for the wing. This effect is believed to be due to the emergence of the tail from an area where large variations of downwash angle with angle of attack occur, as will be discussed in a later section of this report. These results are not unusual, similar characteristics having been observed in the other flight tests in which the tail was located in the plane of the wing chord (see, e.g., refs. 1 to 4).

For Mach numbers less than about 1.0, the maximum lift of the total wing occurred at about 24° angle of attack, the values of $C_{L_{max}}$ ranging from about 0.9 to 1.1 as the Mach number increased from 0.84 to 1.0. At some of the Mach numbers it was necessary to extrapolate the lift curves for the total wing on the basis of exposed-wing data in order to define the values noted above. At Mach numbers greater than 1.0, the maximum lift coefficient was not attained at the highest test angles of attack of 21° to 24°. Some irregularities in the lift curves that occur at values below $C_{L_{max}}$ for the lower test Mach numbers indicate that, as frequently occurs with airplanes, stall characteristics may limit the usable lift coefficients to values below those quoted above.

Drag

In figure 8 the flight variation of minimum drag coefficient with Mach number for the complete model is compared with the theoretical variation computed by adding to the experimental subsonic value the increment determined by the method described in reference 10. The computed transonic drag rise is seen to be in excellent agreement with the experimental transonic drag rise.

In figure 9 the experimental drag rise with lift, expressed in terms of the factor $\partial C_D/\partial C_L^2$ is compared with values computed with the assumption of (1) an elliptic spanwise distribution of lift with full leading-edge suction at subsonic speeds ($\partial C_D/\partial C_L^2 = 1/\pi A$), with modifications to the value of $1/\pi A$ according to linear theory for Mach numbers greater than 1.0; and (2) no leading-edge suction so that the resultant-force vector due to angle of attack is perpendicular to the wing chord ($\partial C_D/\partial C_L^2 = 1/(57.3\ C_{L_\alpha})$). Average low-lift values of C_{L_α} were used in the expression $1/(57.3\ C_{L_\alpha})$. The results for the wing show a slight

but generally progressive decrease in value of $\partial C_D/\partial C_L^2$ with increasing Mach number through the test range (figs. 9(b) and 9(c)). This variation is qualitatively similar to that of the aspect-ratio-3 triangular wing of reference 4, but is different from that experienced with the unswept wing of reference 1 and the aspect-ratio-4 triangular wing of reference 3. The position of the experimental curves in relation to the respective theoretical curves indicates the proportion of leading-edge suction developed. Except at Mach numbers of about 0.96, where an increase in leading-edge suction occurs, the variation in percent of leading-edge suction with Mach number for the wing is small.

Reference 11 shows the considerable effect that Reynolds number may have on the value of $\partial C_D/\partial C_L^2$, the value decreasing with increasing Reynolds number at any particular Mach number. In the present tests the Reynolds number varied simultaneously with the Mach number in each drop (fig. 3). The particular variations for the drop that defined the curves of $\partial C_D/\partial C_L^2$ are shown as supplementary scales in figure 9. Because of this simultaneous variation it is impossible from these tests to state with certainty whether Mach number or Reynolds number is the determining factor. However, since the flow perpendicular to the leading edge of the wing remains at relatively low subsonic speeds through the test range of Mach numbers, it appears more likely that Reynolds number is the fundamental variable that defines the trend of the test results.

Some further evidence that the Reynolds number is the important parameter in defining the variation of $\partial C_D/\partial C_L^2$ is obtained from the characteristics of swept circular cylinders presented in reference 12. As shown in figure 18(a), the minimum pressure coefficient obtained on these cylinders can be related to the Reynolds number based on the cylinder radius and the velocity perpendicular to the cylinder; for each sweep angle there is a critical Reynolds number for the cylinder below which laminar separation, and therefore the smaller peak pressures, occurs. From an examination of figure 18(b), in which the percentage of leading-edge suction[1] is plotted for a family of triangular wings, it can be reasoned that a similar trend exists. Thus the low value of leading-edge suction occurring on the aspect-ratio-4 wing can be explained by the fact that the Reynolds number based on leading-edge radius is in the range where figure 18(a) indicates that laminar separation occurs on the cylinder. In contrast the variations

[1]"Percent leading-edge suction" as used in figure 18(b) is obtained from:

$$\text{Percent leading-edge suction} = \frac{\left(\frac{\partial C_D}{\partial C_L^2}\right)_{1/(57.3\,C_{L_\alpha})} - \left(\frac{\partial C_D}{\partial C_L^2}\right)_{\text{test}}}{\left(\frac{\partial C_D}{\partial C_L^2}\right)_{1/(57.3\,C_{L_\alpha})} - \left(\frac{\partial C_D}{\partial C_L^2}\right)_{1/\pi A}}$$

where the subscripts define the curves from which the values of $(\partial C_D/\partial C_L^2)$ are obtained.

of leading-edge suction obtained on the aspect-ratio-2 and -3 wings correspond qualitatively with the variations of minimum-pressure coefficient that characterize the transition Reynolds number for the 60° swept cylinder in figure 18(a). The generality of this result, particularly with regard to the Mach number range over which it applies, has not yet been demonstrated; a similar analysis applied to data from other sources correlates in some cases but fails to correlate in others.

Static Longitudinal Stability

In figure 19 the variations of aerodynamic-center position with Mach number for the wing at low lift coefficients are compared with the variations measured on wings of similar plan form in other test facilities (refs. 6, 13, and 14). The aerodynamic center moves aft about 6-percent $\bar{c}$ in traversing the transonic Mach number range, about the same movement indicated by the wind-tunnel data. The flight data differ somewhat from the wind-tunnel values, however, in that the flight values are as much as 9-percent $\bar{c}$ aft of the wind-tunnel values at comparable Mach numbers. Also, the flight variation with Mach number is not entirely progressive, a slight forward movement with increasing Mach number occurring at about M = 1.0. The reasons for these differences are not known.

Insofar as the variation of aerodynamic-center position with angle of attack for the wing is concerned, there appeared to be little movement over the unstalled range of angles of attack. This is indicated by the linearity of the curves of figure 11, as well as by the small difference in values indicated between the curves for $\alpha = 0^\circ$ and $\alpha = 10^\circ$ in figure 12.

The stability contribution of the tail was small at small angles of attack throughout the test Mach number range (figs. 10(b) and 12). The range of angles of attack through which the tail contribution remained small appeared to increase progressively with increasing Mach number throughout the test range of Mach numbers. This result is in contrast with the findings of the other wings of the flight-test program, which indicated similar reductions in tail contribution at small angles of attack, but which showed the greatest extent of angle of attack for reduced tail contribution to be at Mach numbers of the order of 0.92 (refs. 1, 3, and 4). It is noteworthy in this regard that the present wing has a lower aspect ratio and greater sweep of the leading edge than any of the other wings, but there is insufficient evidence to permit the causes of the differences to be stated.

Wind-tunnel data for wings similar to those of references 1, 3, and 4 indicated that the aforementioned reduction in tail contribution was due to a large variation of downwash angle with angle of attack. There are no comparable wind-tunnel data for the present wing, but the indications are that the same factor is the cause.

Dynamic Longitudinal Stability

The results of figure 13 show that values of the damping-in-pitch parameter $C_{m_q} + C_{m_{\dot{\alpha}}}$ are somewhat greater than values estimated for the fuselage plus the tail in the presence of the wing. The contribution of the tail was estimated as described in reference 8 using a value of $\partial\epsilon/\partial\alpha$ of 0.5. In view of the preceding discussion that indicated the existence of much higher values of $\partial\epsilon/\partial\alpha$ at small angles of attack, a higher value of $\partial\epsilon/\partial\alpha$ should probably have been used in the calculation which would have increased the magnitudes of the estimated values of $C_{m_q} + C_{m_{\dot{\alpha}}}$. However, further refinements of this kind were considered unwarranted in view of the nonlinearity of the variation of ϵ with α and the fact that each value of $C_{m_q} + C_{m_{\dot{\alpha}}}$ was determined from several cycles of data, each of which covered a different range of angles of attack.

Some values of $C_{m_q} + C_{m_{\dot{\alpha}}}$ are shown in reference 15 for a wing of the same plan form as the test wing. Addition of the increment for the wing as obtained from reference 15 to the estimated values for the fuselage and tail seems to improve the agreement with the flight data in figure 13; this agreement may, however, be fortuitous in view of the uncertainty as to the estimated curve for the fuselage plus tail as previously discussed.

Horizontal-Tail Effectiveness

In figure 14 values of the horizontal-tail effectiveness parameter C_{m_δ} are compared with values obtained in other tests in which the same tail was mounted behind wings of other plan form. The comparison indicates a slightly lower effectiveness for the tail at small angles of attack in the present tests as compared with the results from references 1, 3, 4, and 8. This difference results from a lower dynamic pressure at the tail for this wing as compared with the other wings.

SUMMARY OF RESULTS

Flight tests at transonic speeds of a free-falling model incorporating a triangular wing of aspect ratio 2 and a 45° swept horizontal tail in the chord plane of the wing showed the following results:

1. The aerodynamic center of the wing varied with Mach number in a manner similar to that shown by wind-tunnel tests, but the locations were as much as 9 percent of the mean aerodynamic chord further aft than in the wind-tunnel tests.

2. The experimental increase in minimum drag for the complete model through the transonic Mach number range was closely predicted by use of available methods.

3. The drag-rise-with-lift factor for the wing decreased generally with increasing Mach number and simultaneously increasing Reynolds number throughout the transonic speed range.

4. A similarity was noted between the Reynolds numbers (based on the leading-edge radius) at which the drag-rise-with-lift factor changed rapidly for a family of triangular wings, and the Reynolds numbers at which the pressures over swept circular cylinders changed due to differences in boundary-layer separation.

5. A large variation of downwash angle with angle of attack at small angles of attack that had been reported in other tests of tails mounted in the chord plane of low-aspect-ratio wings was also indicated in the present investigation. The range of angles of attack over which this effect was observed increased progressively with increasing Mach number.

Ames Aeronautical Laboratory
National Advisory Committee for Aeronautics
Moffett Field, Calif., June 21, 1955

REFERENCES

1. White, Maurice D.: A Flight Investigation at Transonic Speeds of the Aerodynamic Characteristics of a Model Having a Thin Unswept Wing of Aspect Ratio 3.1. NACA RM A54E12, 1954.

2. Holdaway, George H.: A Flight Investigation at Transonic Speeds and Small Angles of Attack of the Aerodynamic Characteristics of a Model Having a 45° Sweptback Wing of Aspect Ratio 3 With an NACA 64A006 Airfoil Section. NACA RM A54I17, 1955.

3. Bright, Loren G.: A Flight Investigation at Transonic Speeds of a Model Having a Triangular Wing of Aspect Ratio 4. NACA RM A54L27, 1955.

4. White, Maurice D.: A Flight Investigation at Transonic Speeds of a Model Having a Triangular Wing of Aspect Ratio 3. NACA RM A55D18, 1955.

5. Hall, Charles F.: Lift, Drag, and Pitching Moment of Low-Aspect-Ratio Wings at Subsonic and Supersonic Speeds. NACA RM A53A30, 1953.

6. Emerson, Horace F., and Gale, Bernard M.: Transonic Aerodynamic Characteristics of Three Thin Triangular Wings and a Trapezoidal Wing, All of Low Aspect Ratio. NACA RM A52D21, 1952.

7. Holdaway, George H.: Comparison of the Aerodynamic Characteristics at Transonic Speeds of a Plane Wing and a Cambered and Twisted Wing, Both Having 45° of Sweepback and an Aspect Ratio of 6. NACA RM A53B16, 1953.

8. White, Maurice D.: Effect of Camber and Twist on the Stability Characteristics of Models Having a 45° Swept Wing as Determined by the Free-Fall Method at Transonic Speeds. NACA RM A52F16, 1952.

9. Brown, Clinton E., and Michael, William H., Jr.: On Slender Delta Wings With Leading-Edge Separation. NACA TN 3430, 1955.

10. Holdaway, George H.: Comparison of Theoretical and Experimental Zero-Lift Drag-Rise Characteristics of Wing-Body-Tail Combinations Near the Speed of Sound. NACA RM A53H17, 1953.

11. Polhamus, Edward C.: Drag Due to Lift at Mach Numbers Up to 2.0. NACA RM L53I22b, 1953.

12. Bursnall, William J., and Loftin, Laurence K., Jr.: Experimental Investigation of the Pressure Distribution About a Yawed Circular Cylinder in the Critical Reynolds Number Range. NACA TN 2463, 1951.

13. Smith, Donald W., and Heitmeyer, John C.: Lift, Drag, and Pitching Moment of Low-Aspect-Ratio Wings at Subsonic and Supersonic Speeds - Plane Triangular Wing of Aspect Ratio 2 With NACA 0005-63 Section. NACA RM A50K21, 1951.

14. Heitmeyer, John C., and Smith, Willard G.: Lift, Drag, and Pitching Moment of Low-Aspect-Ratio Wings at Subsonic and Supersonic Speeds - Plane Triangular Wing of Aspect Ratio 2 With NACA 0003-63 Section. NACA RM A50K24a, 1951.

15. Tobak, Murray: Damping in Pitch of Low-Aspect-Ratio Wings at Subsonic and Supersonic Speeds. NACA RM A52L04a, 1953.

TABLE I.- DIMENSIONS OF FREE-FALL MODEL

Gross weight, lb	1860 and 1700
Moment of inertia about Y axis, slugs-ft^2	1000 and 977
Center of gravity	0.397 and 0.467$\bar{c}$
Wing	
Area, sq ft	30.3
Area, exposed panels, sq ft	20.9
Aspect ratio	2.0
Taper ratio	0
Span, ft	7.79
Mean aerodynamic chord, ft	5.19
Airfoil section, parallel to stream	NACA 0005-63
Horizontal tail (all-movable, pivoting about axis perpendicular to longitudinal axis of model)	
Area (including 2.0 sq ft included in fuselage), sq ft	6.0
Aspect ratio	4.5
Taper ratio	0.20
Span, ft	5.21
Mean aerodynamic chord (including area included in fuselage), ft	1.36
Leading edge of mean aerodynamic chord	Station 153.6
Root chord, ft	1.96
Tip chord, ft	0.40
Airfoil section, parallel to stream	NACA 65006
Gap between tail and fuselage at 0° deflection, in.	1/16
Vertical tail (all-movable differentially, pivoting about axis perpendicular to longitudinal axis of model)	
Area (including 1.4 sq ft included in fuselage), sq ft	3.3
Aspect ratio	5.1
Taper ratio	0.22
Span, ft	4.1
Mean aerodynamic chord (including area included in fuselage), ft	0.93
Leading edge of mean aerodynamic chord	Station 151.0
Root chord, ft	1.34
Tip chord, ft	0.29
Airfoil section, perpendicular to quarter-chord line	NACA 65009
Gap between tail and fuselage at 0° deflection, in.	1/16
Fuselage	
Fineness ratio	12.4
Ordinate at station x(x = 8.0 to x = 139.4), in.	$r = 8.5\left[1 - \left(\frac{x - 102}{102}\right)^2\right]^{3/4}$

TABLE II.- ORDINATES OF WING AIRFOIL SECTION

Station, percent chord	Ordinate, percent chord
0	0
1.25	.789
2.50	1.089
5.00	1.481
7.50	1.750
10.00	1.951
15.00	2.227
20.00	2.391
25.00	2.476
30.00	2.501
40.00	2.418
50.00	2.206
60.00	1.902
70.00	1.527
80.00	1.093
90.00	.603
95.00	.336
100.00	.052
Leading-edge radius:	0.278 percent chord

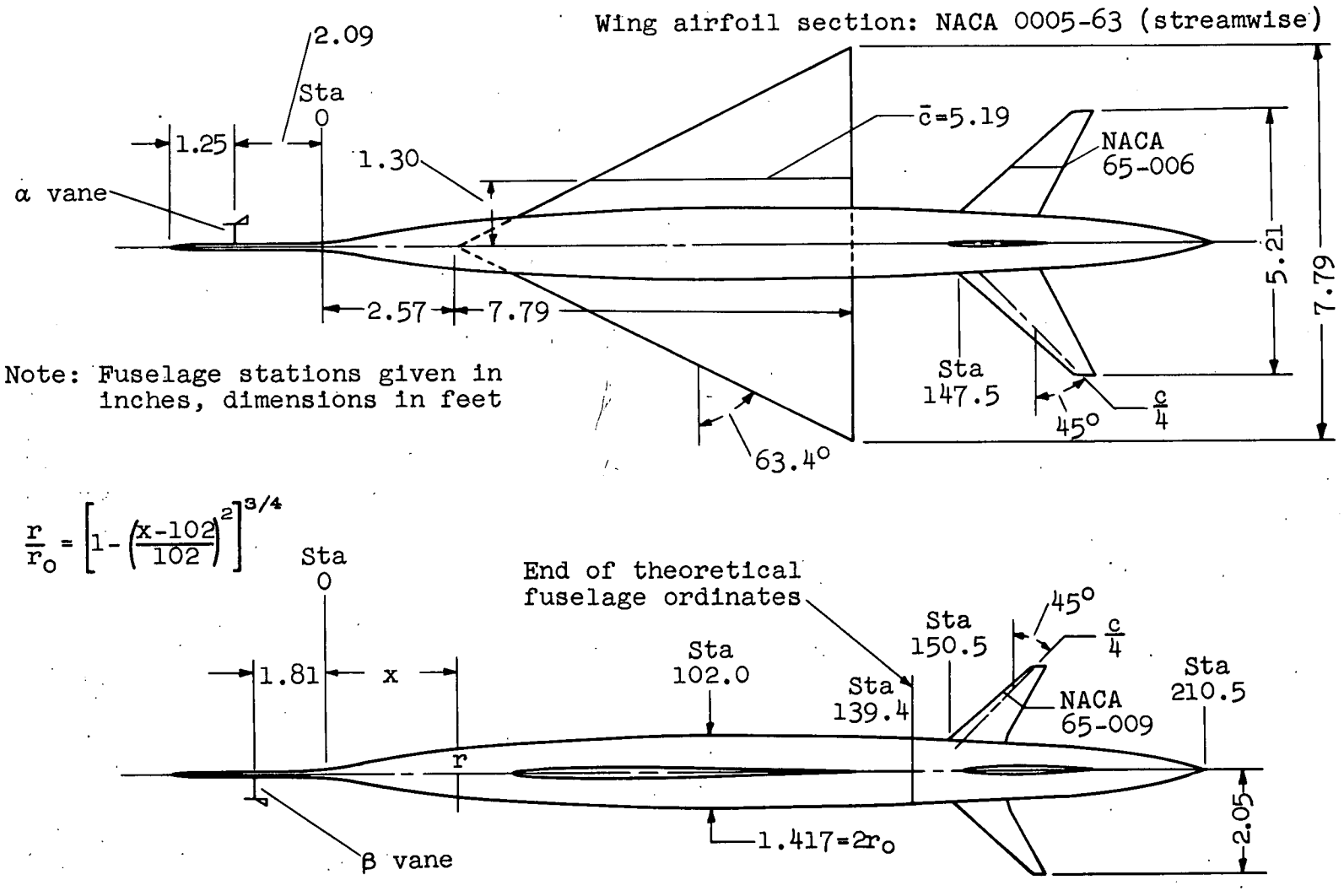

Figure 1.- Dimensional sketch of test model configuration.

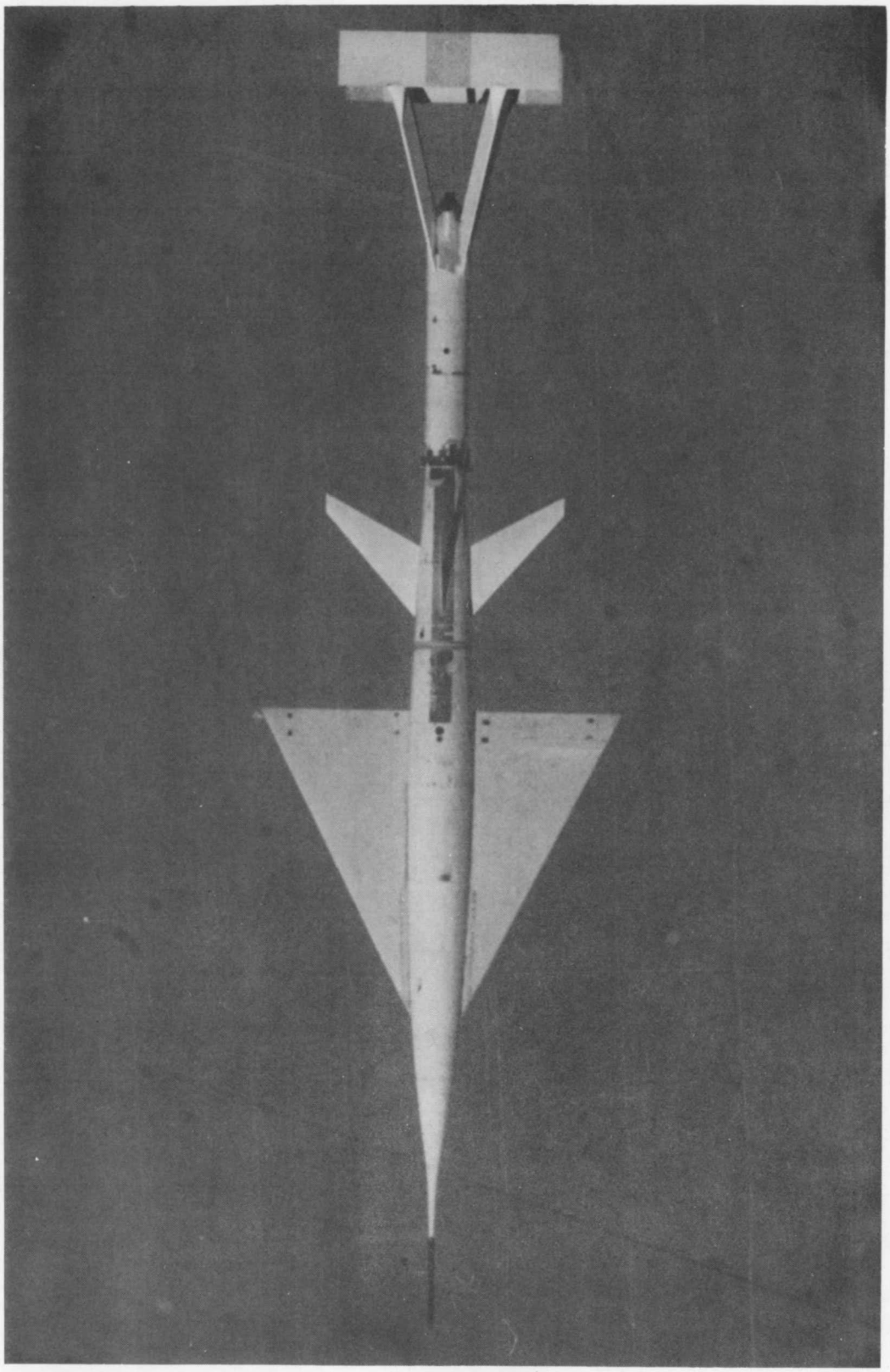

A-19940

Figure 2.- Free-falling recoverable model with aspect-ratio-2 triangular wing and jettisonable booster.

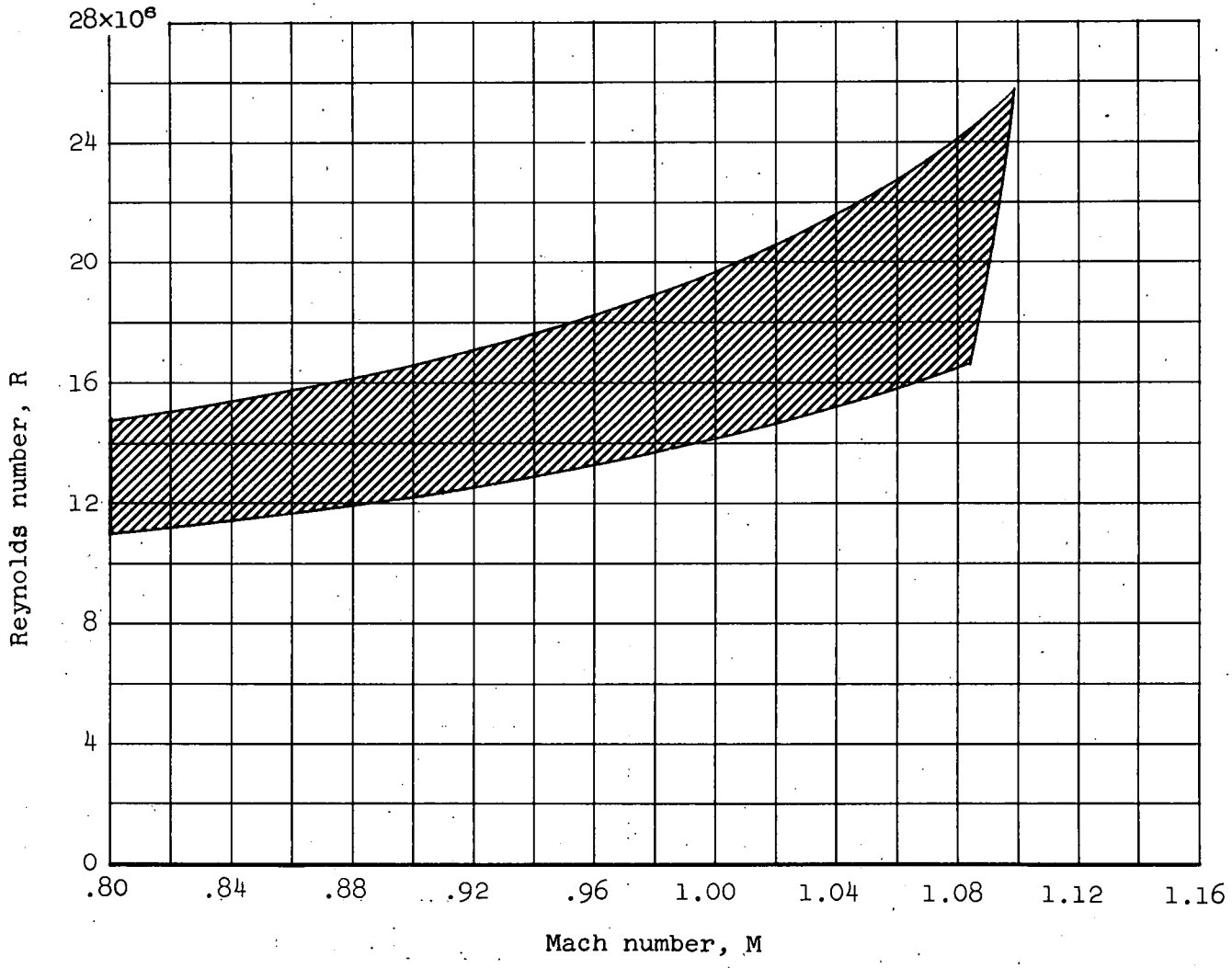

Figure 3.- Variation with Mach number of Reynolds number covered by test program.

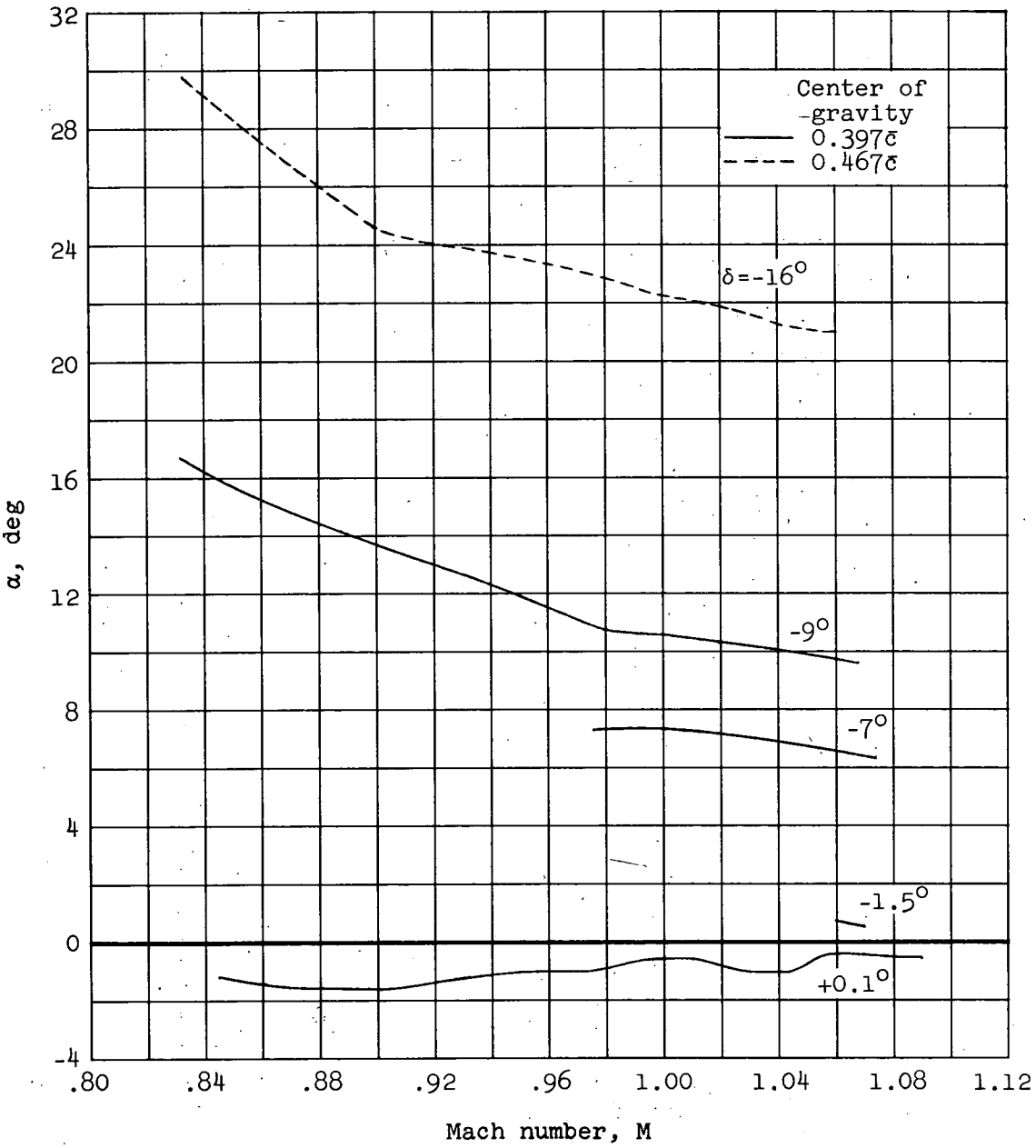

Figure 4.- Variation with Mach number of trim angle of attack for several horizontal-tail settings.

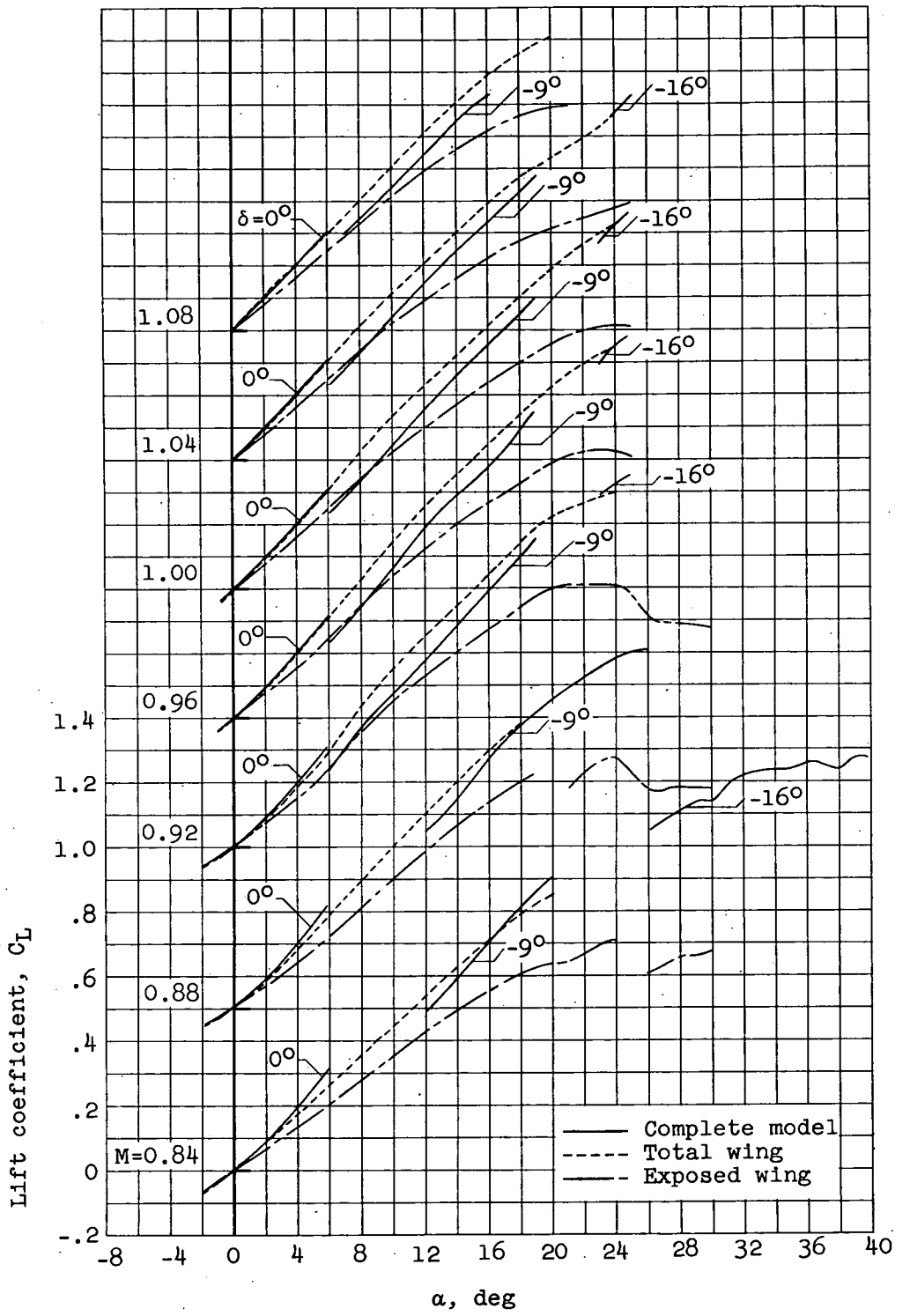

Figure 5.- Lift curves for various components of the test model.

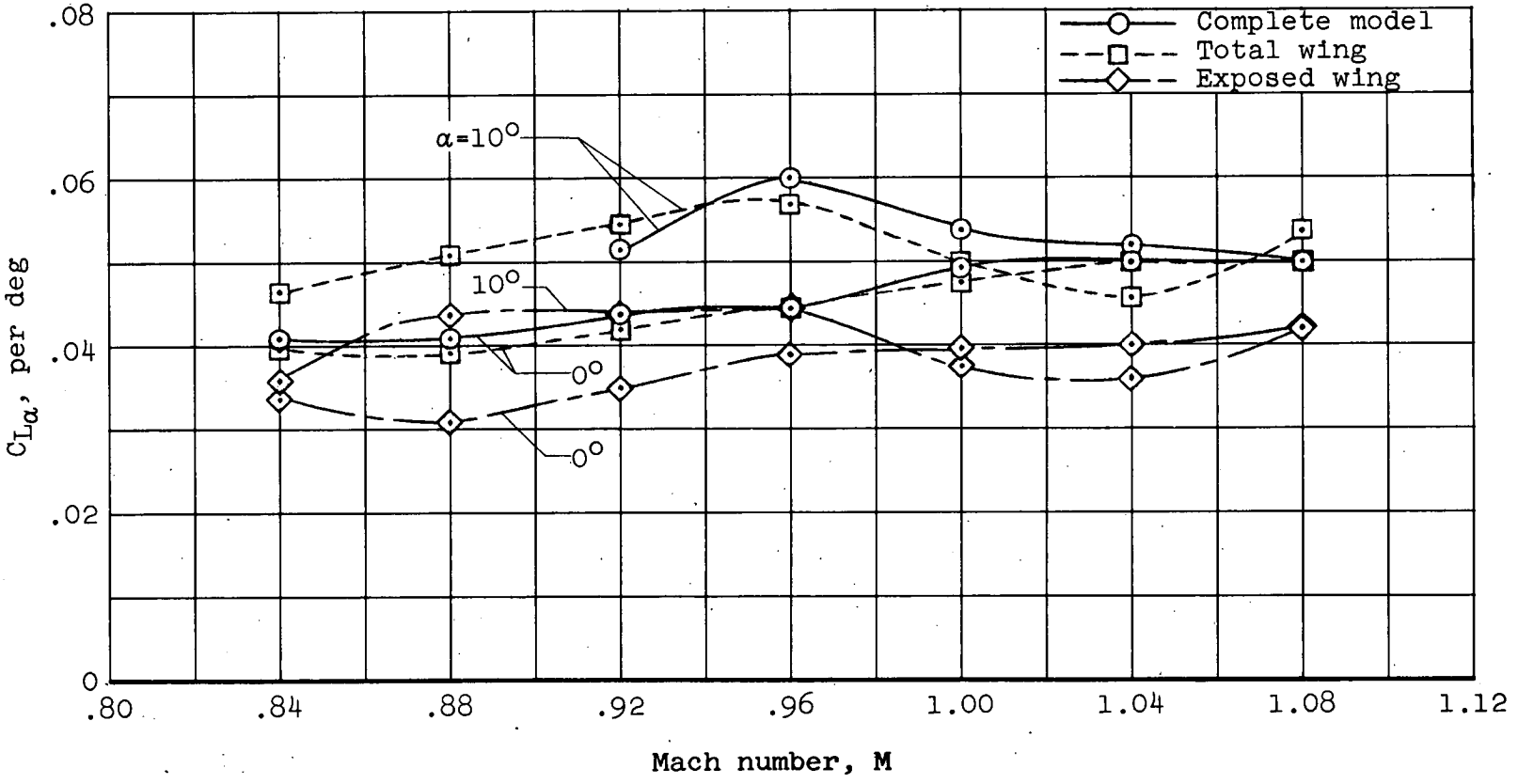

Figure 6.- Variation with Mach number of lift-curve slopes for the components of the test model.

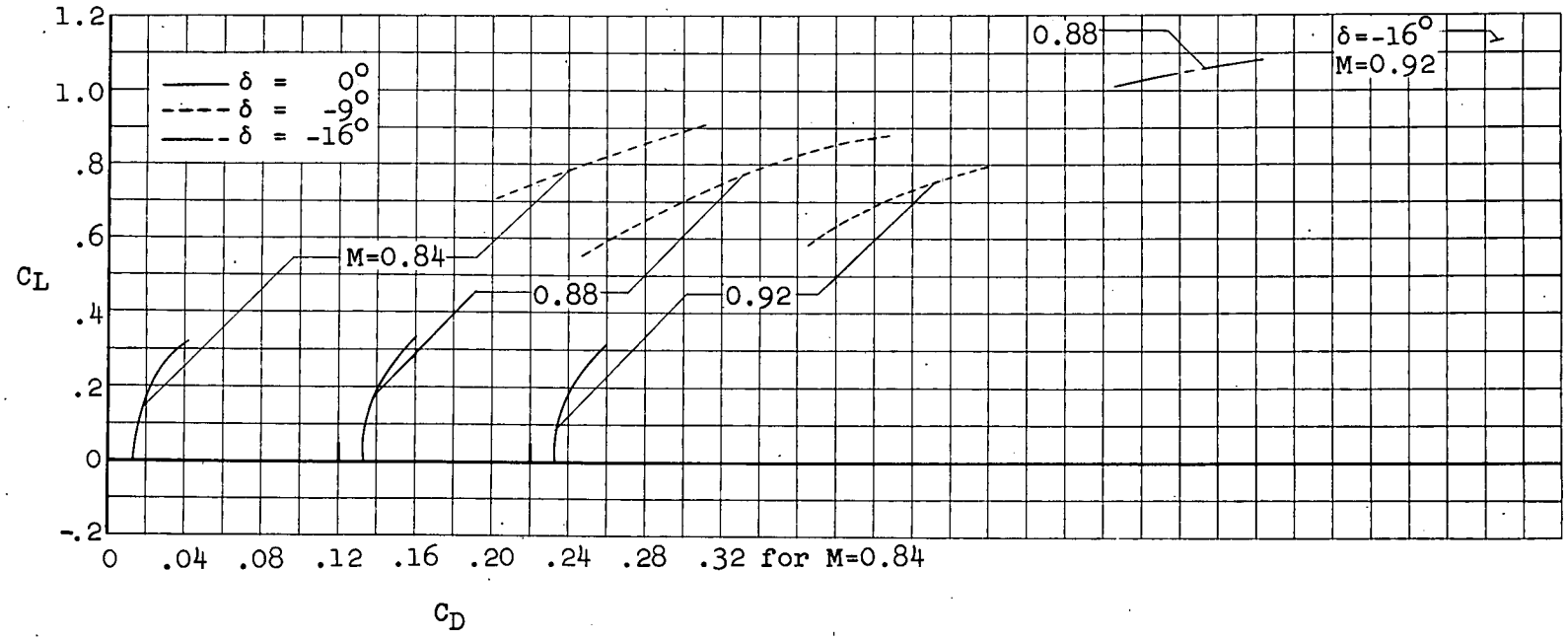

(a) Complete model, M = 0.84 to M = 0.92.

Figure 7.- Variation of drag with lift for the complete model and for the wing at various Mach numbers.

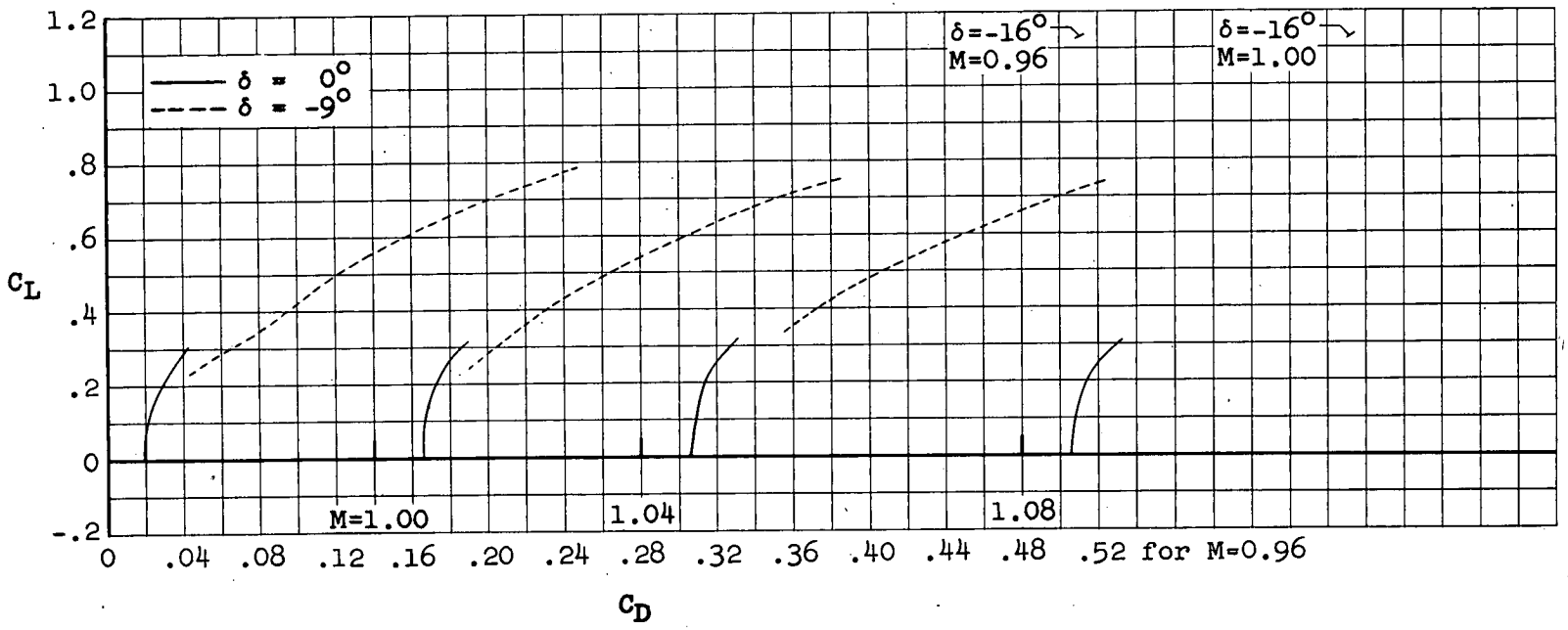

(b) Complete model, M = 0.96 to M = 1.08.

Figure 7.- Continued.

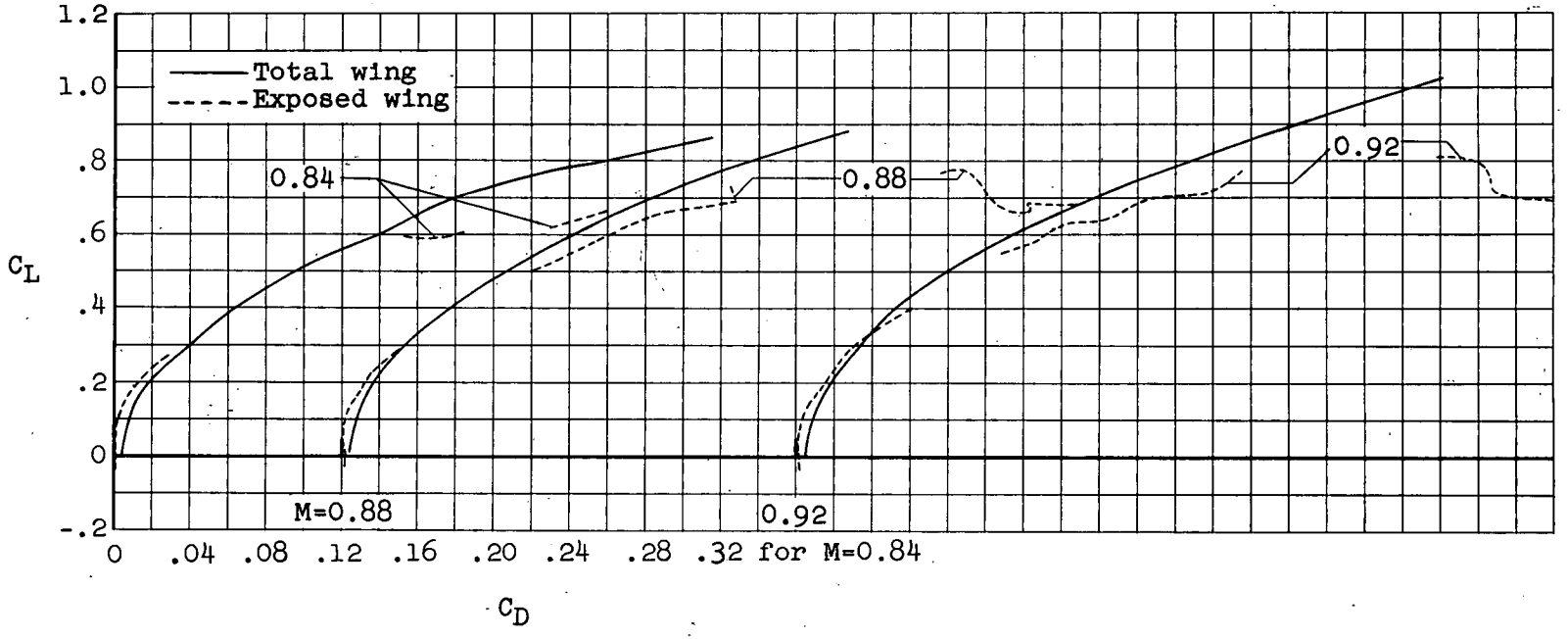

(c) Wing, M = 0.84 to M = 0.92.

Figure 7.- Continued.

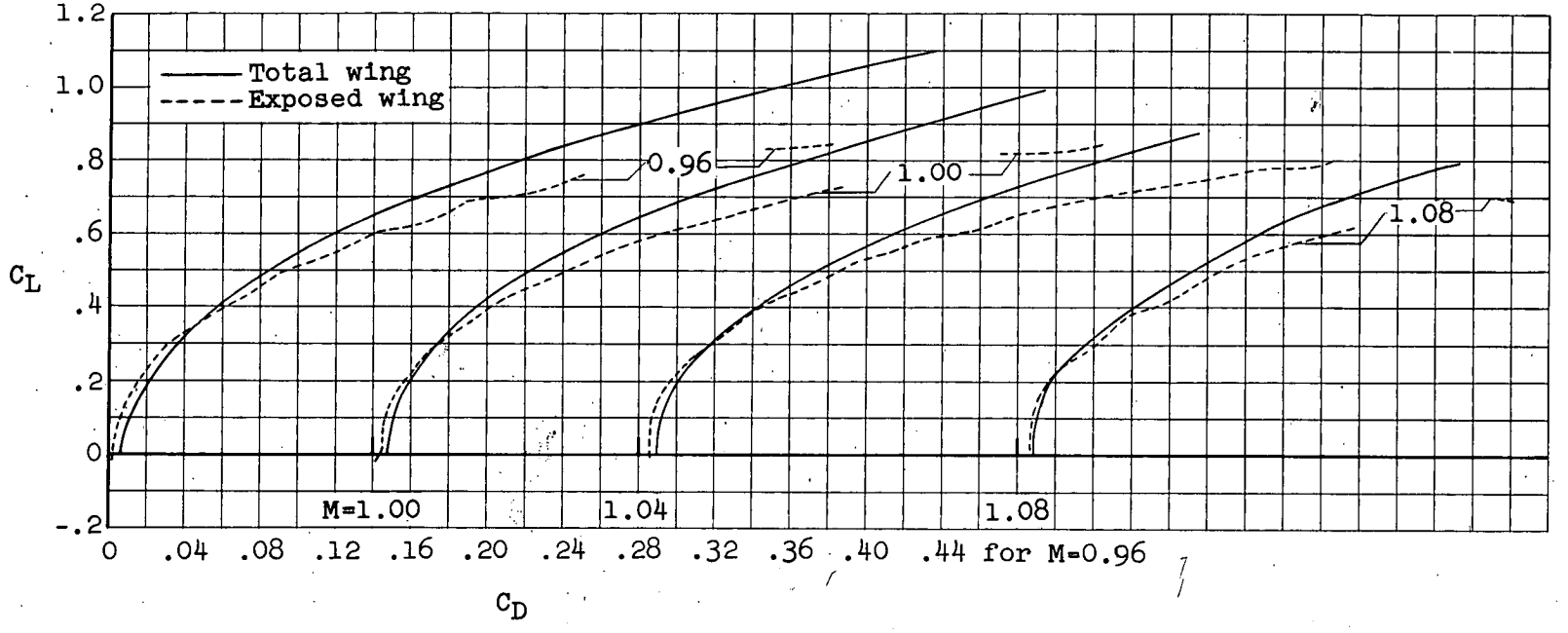

(d) Wing, M = 0.96 to M = 1.08.

Figure 7.- Concluded.

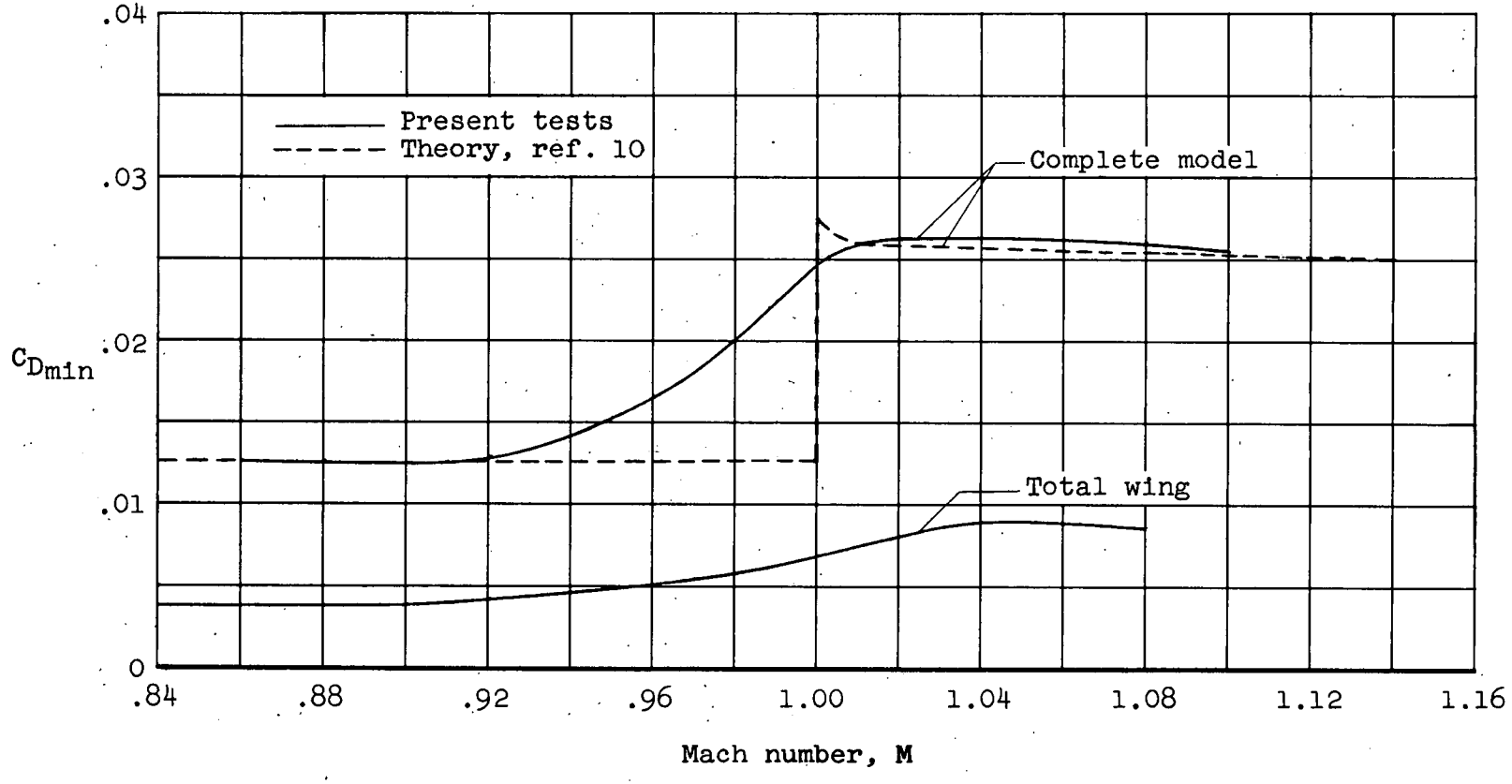

Figure 8.- Variation with Mach number of minimum drag coefficient for the wing and for the complete model.

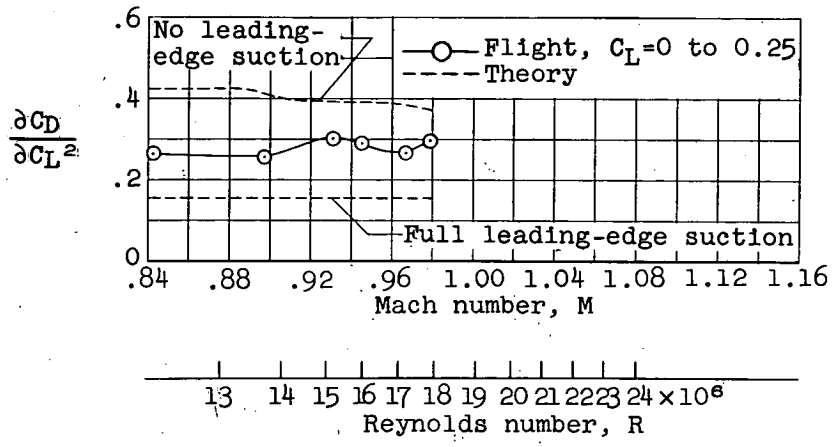

(a) Complete model.

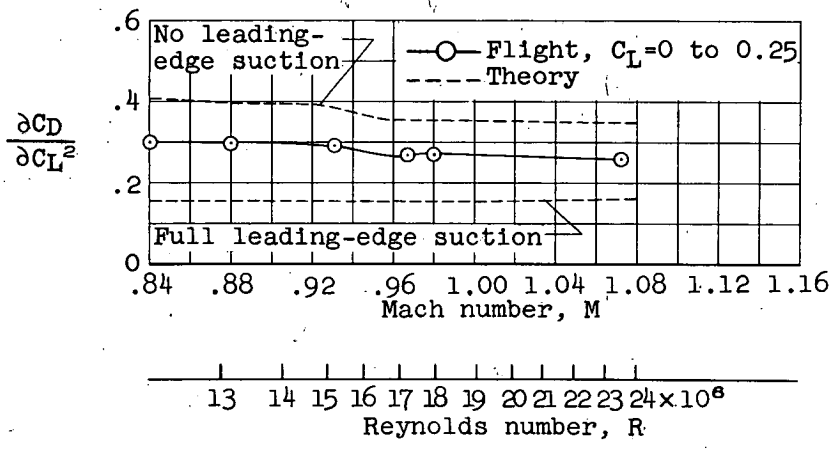

(b) Total wing.

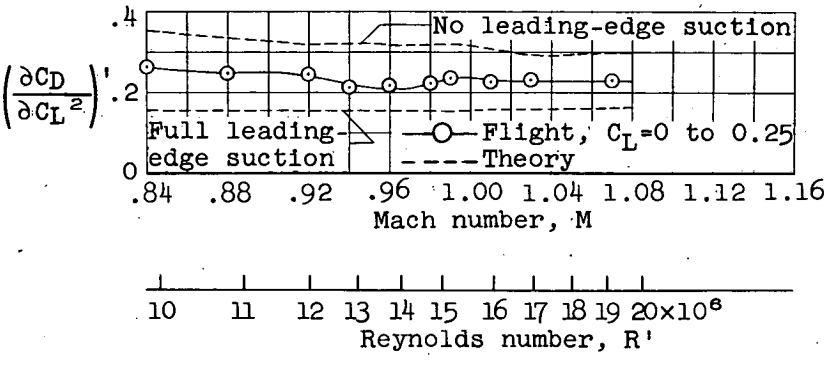

(c) Exposed wing.

Figure 9.- Variation with Mach number of drag-rise factor $\partial C_D/\partial C_L^2$ for the complete model and for the wing. Primed values are based on dimensions of the exposed wing, rather than the total wing.

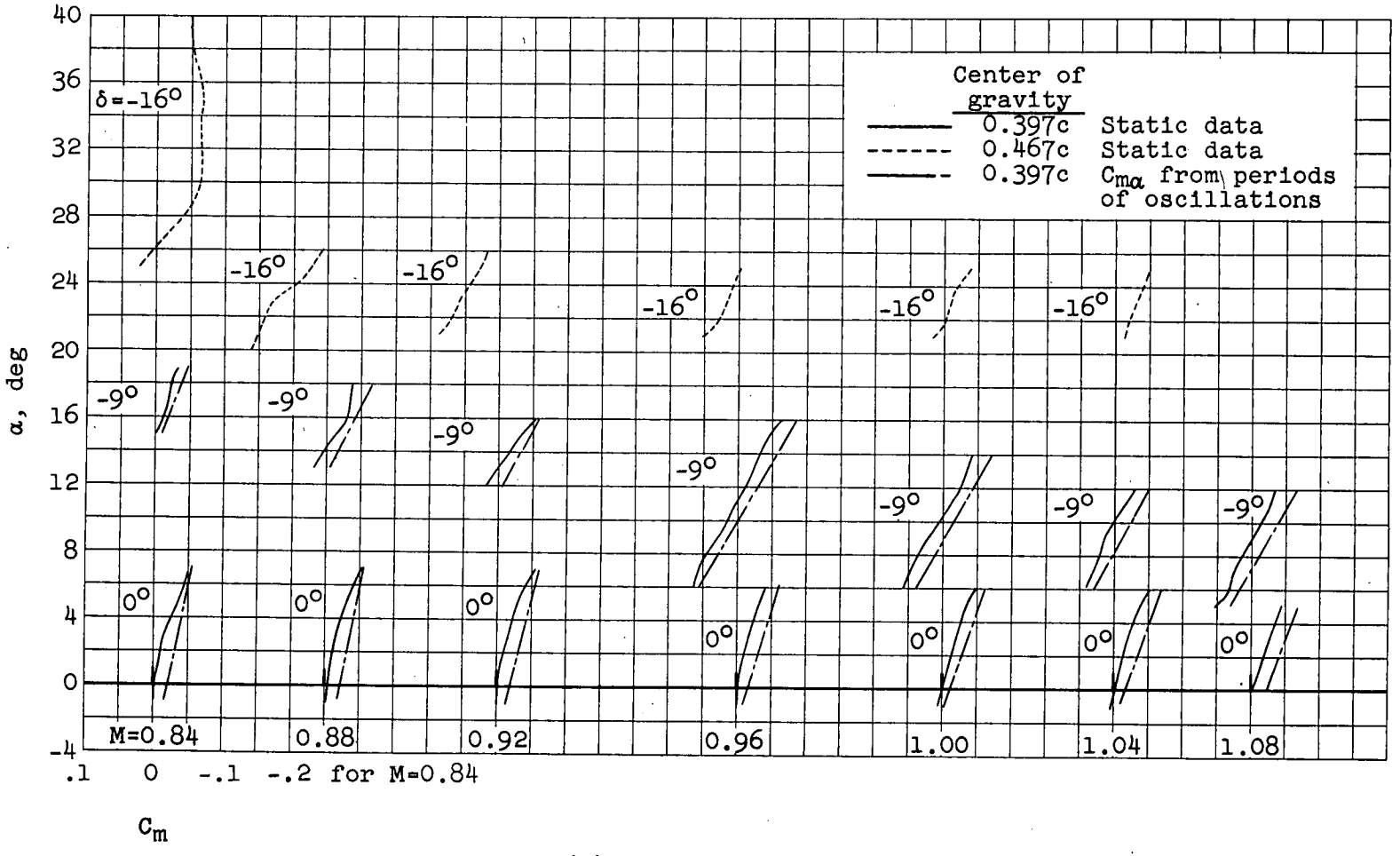

(a) Complete model.

Figure 10.- Variation with angle of attack of pitching-moment coefficients for various components of the test model.

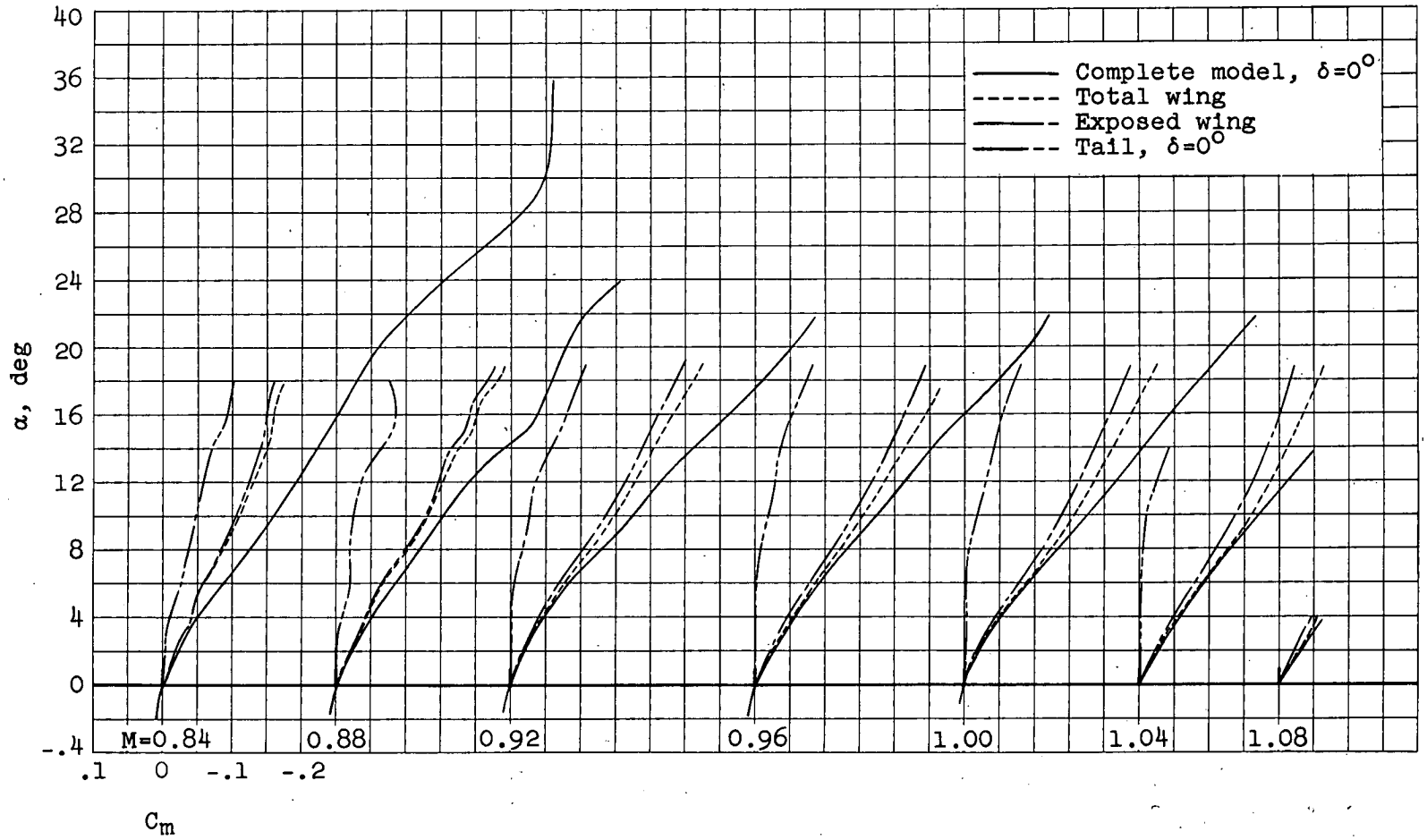

(b) Components of the model; center of gravity at 0.25$\bar{c}$.

Figure 10.- Concluded.

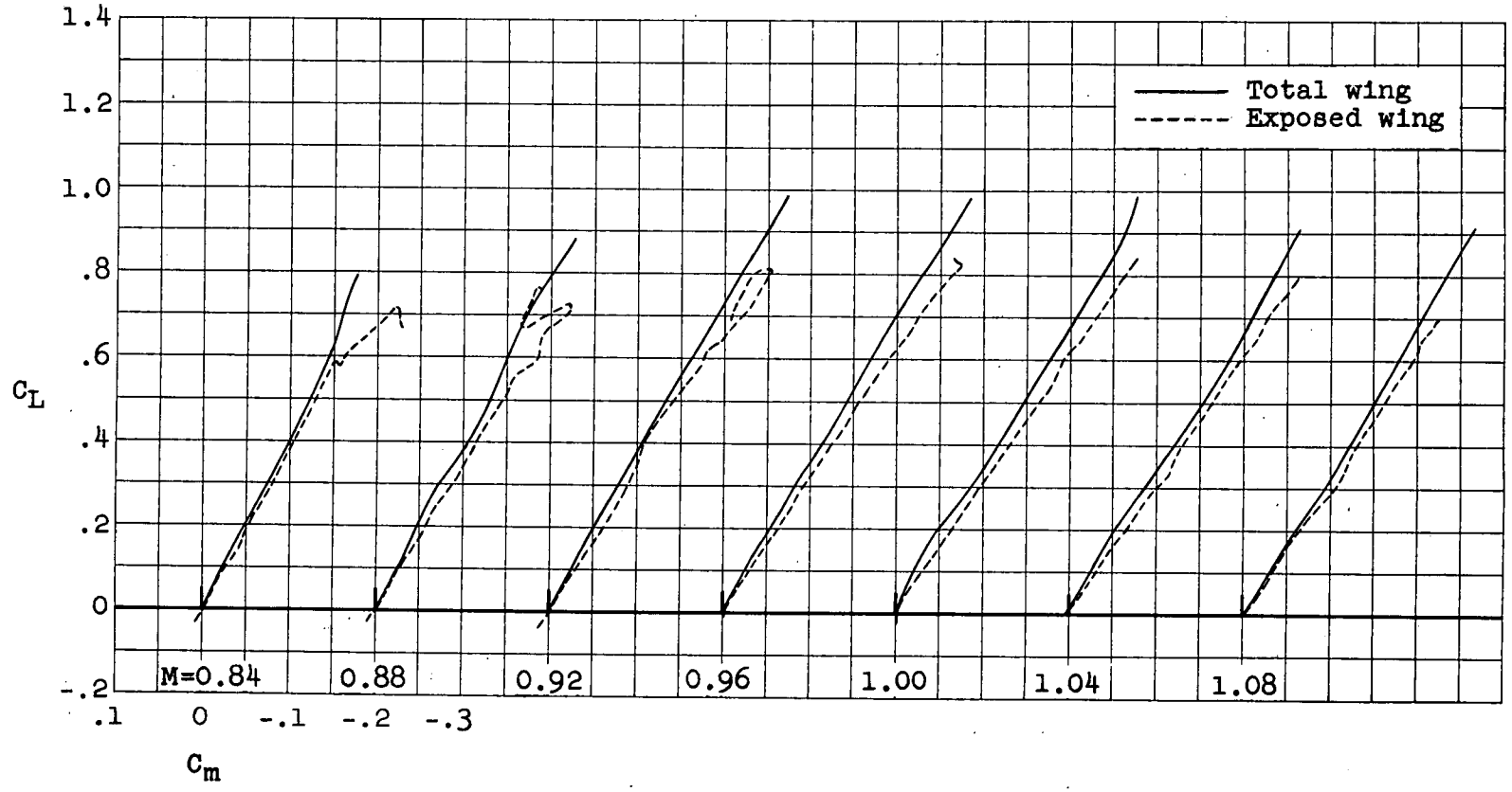

Figure 11.- Variation of pitching-moment coefficient with lift coefficient for wing of model; center of gravity at $0.25\bar{c}$.

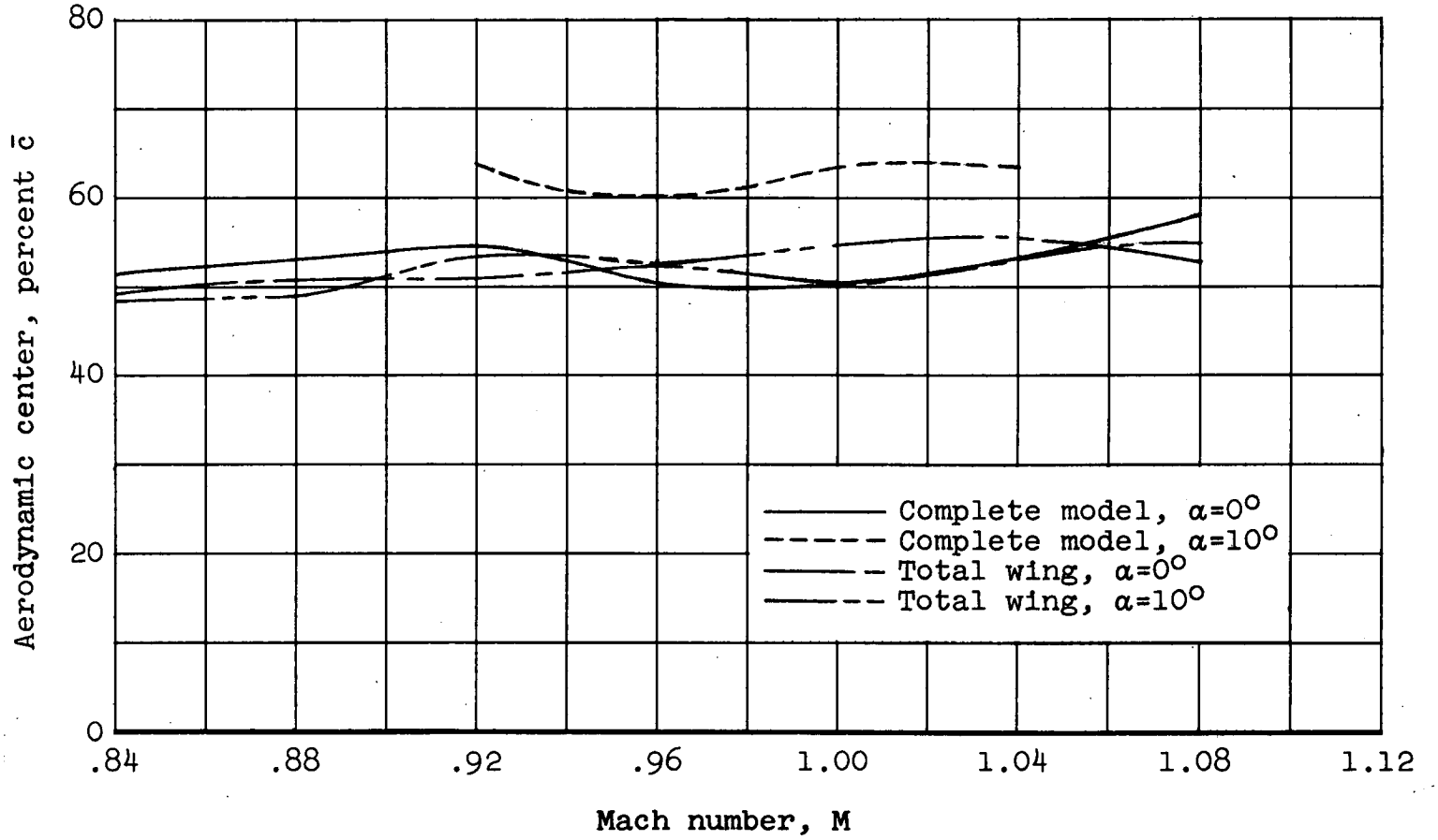

Figure 12.- Variation with Mach number of aerodynamic-center location for the wing and for the complete model.

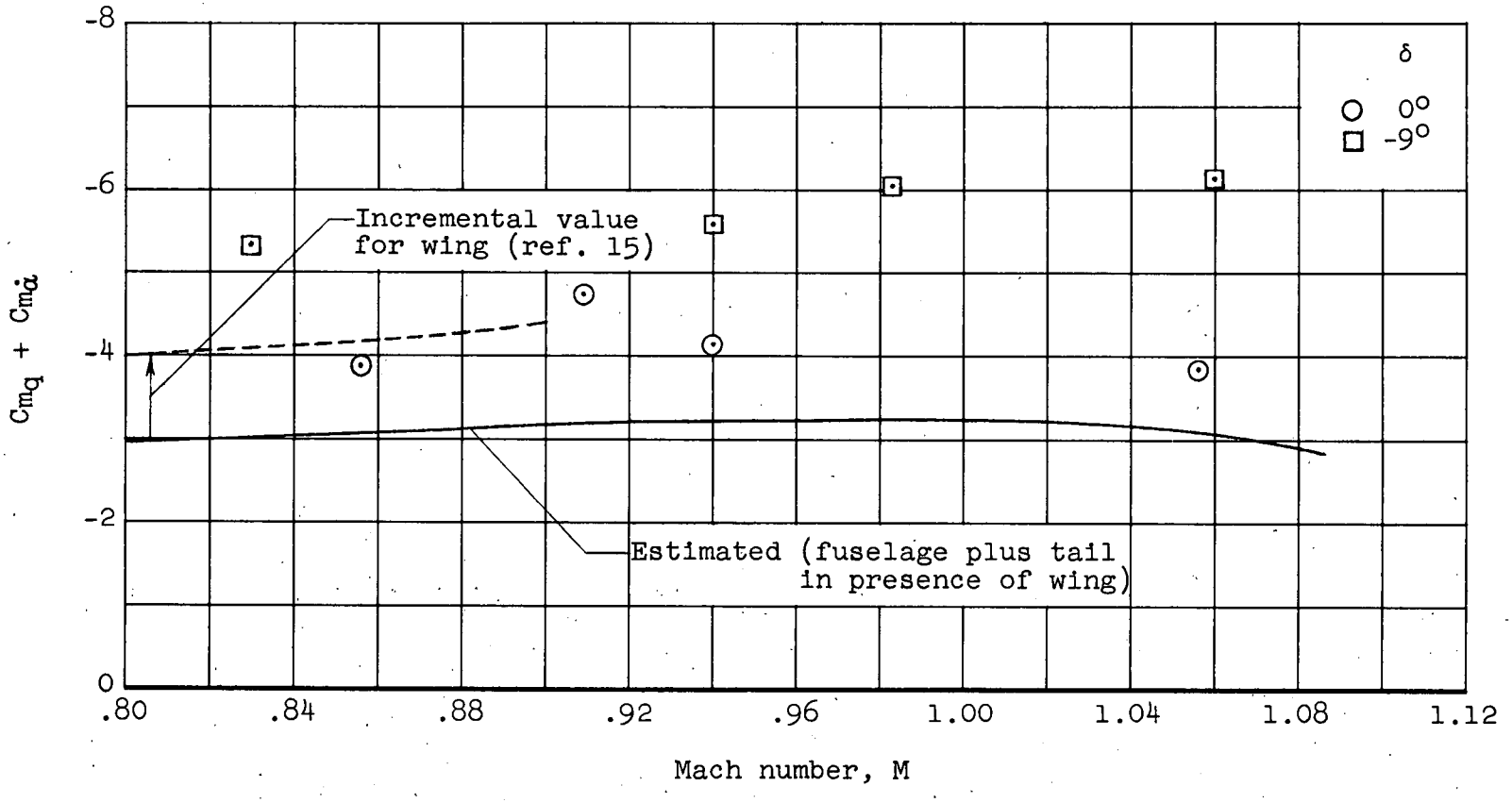

Figure 13.- Variation with Mach number of the damping-in-pitch parameter, $C_{m_q} + C_{m_{\dot{\alpha}}}$.

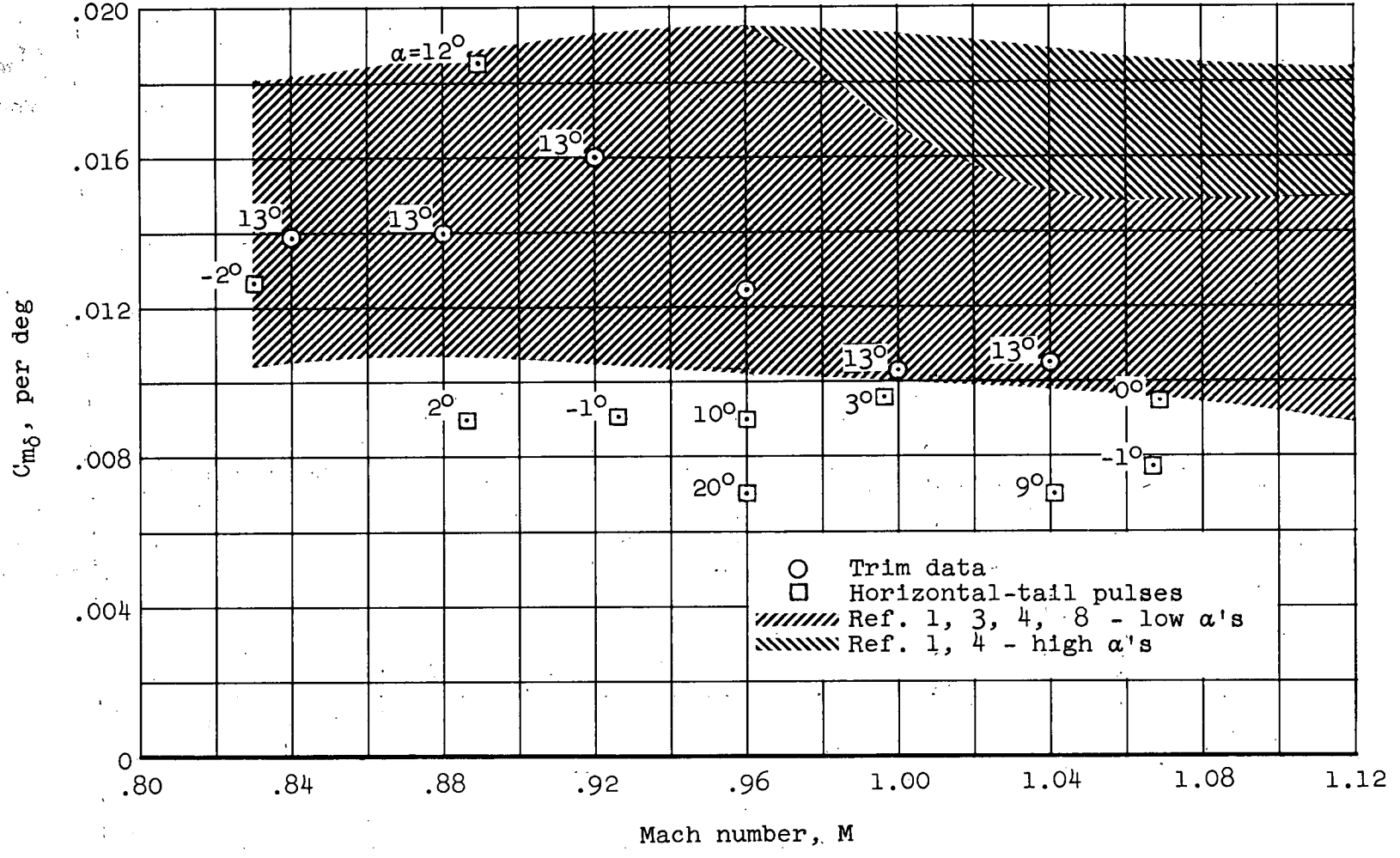

Figure 14.- Variation with Mach number of horizontal-tail-effectiveness parameter, C_{m_δ}; center of gravity at 0.397$\bar{c}$. Values of α noted by data points.

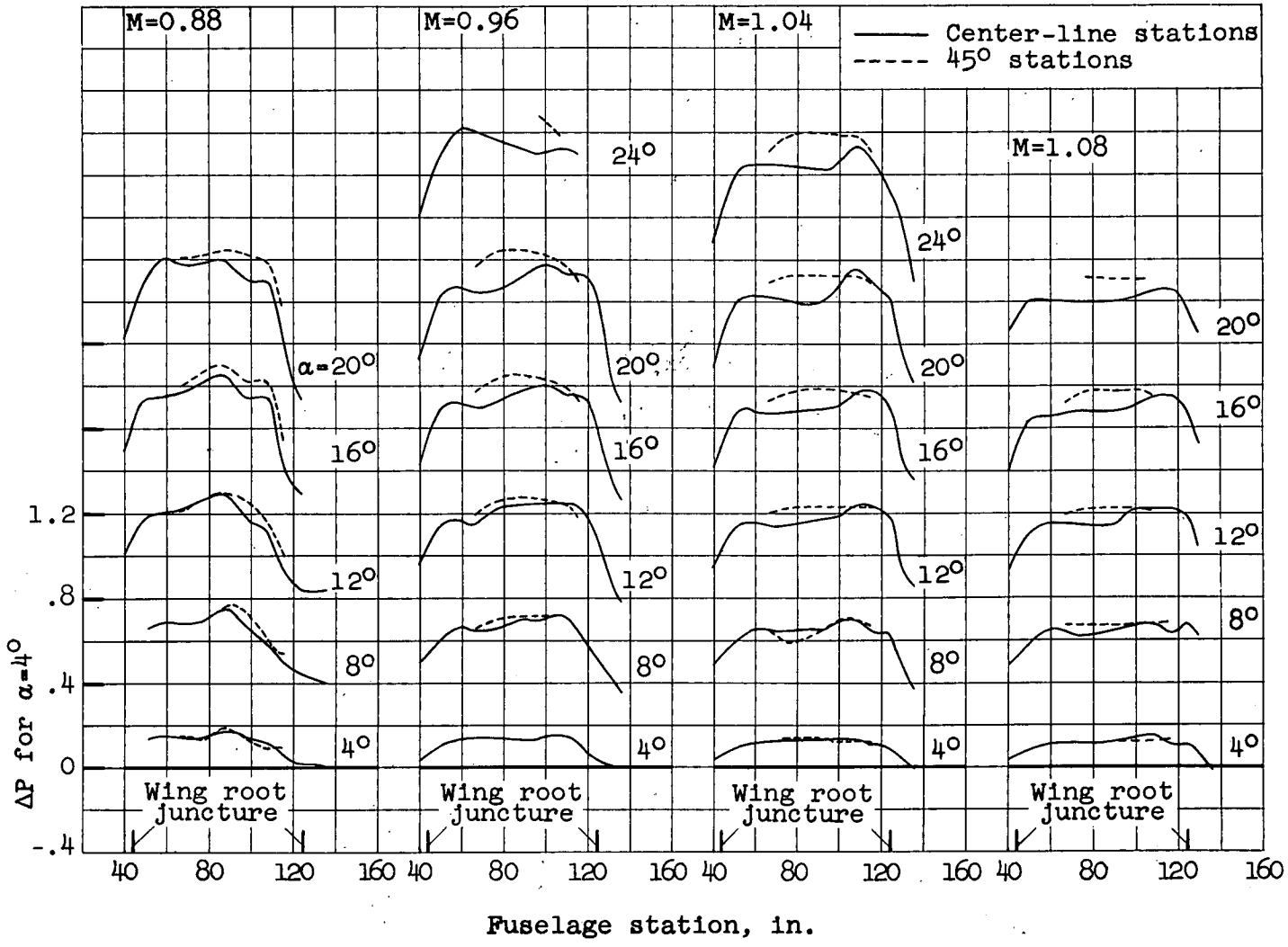

Figure 15.- Loading distribution over the fuselage in the vicinity of the wing.

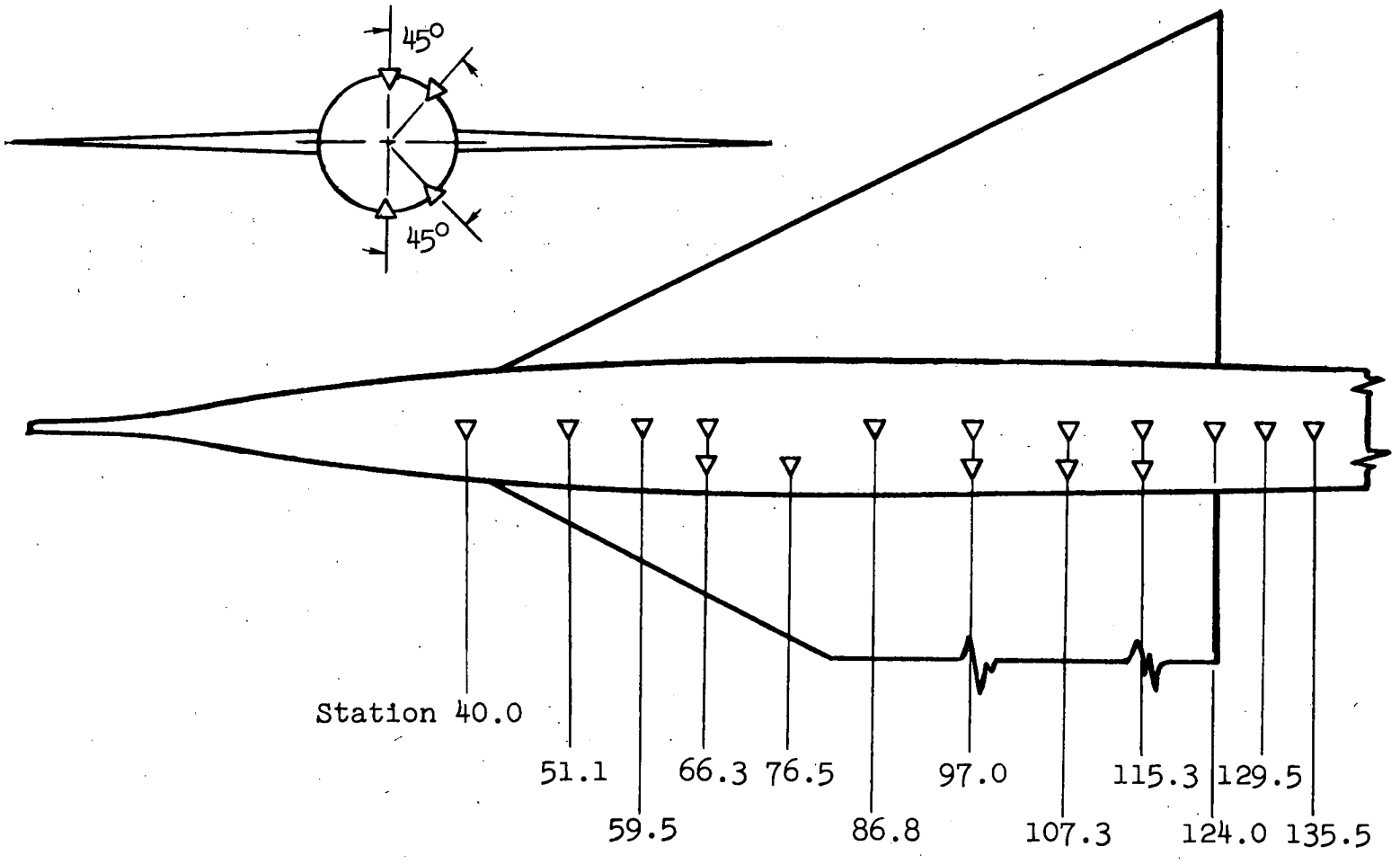

Figure 16.- Locations of pressure orifices on upper and lower surfaces of fuselage.

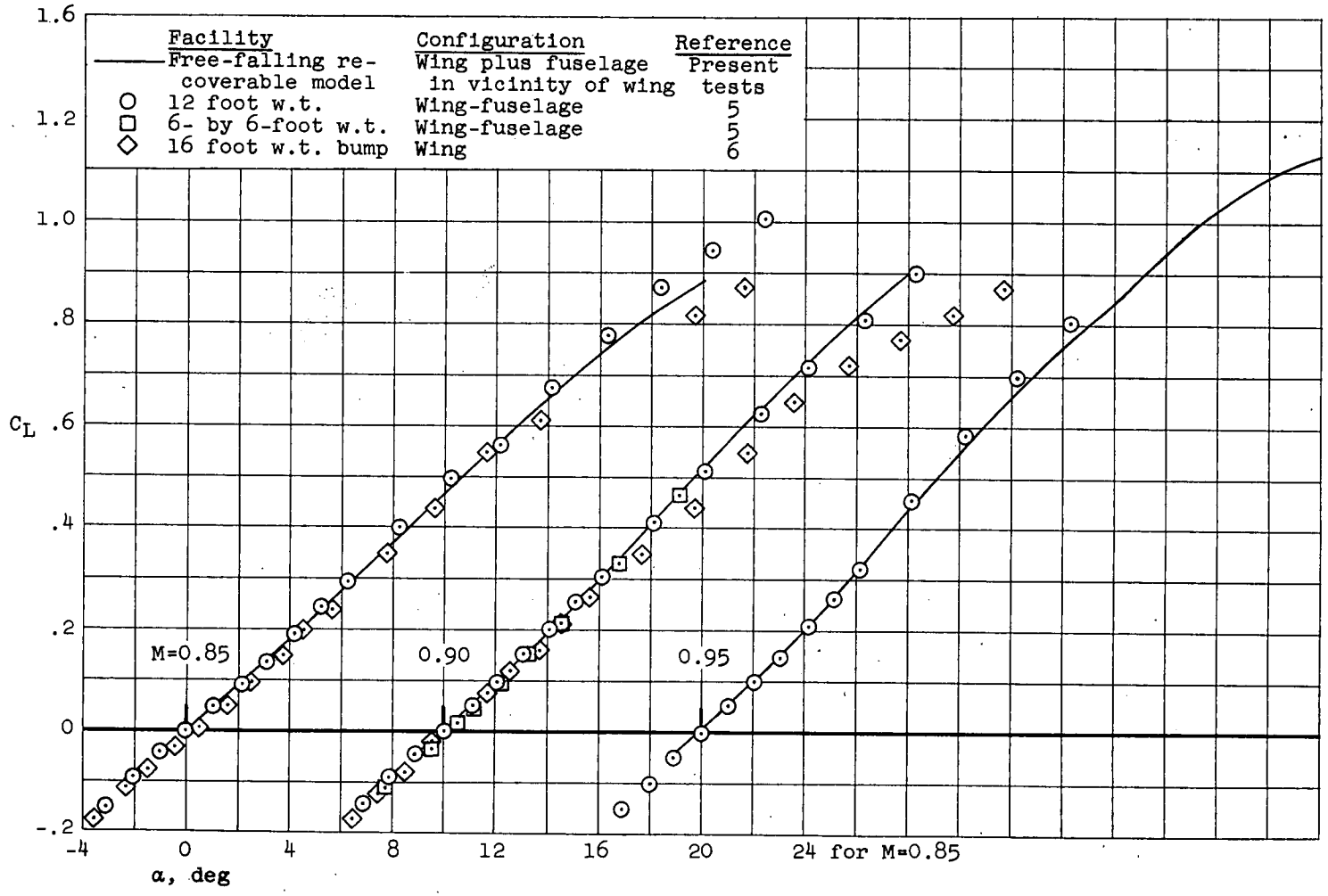

Figure 17.- Comparison of lift curves from flight tests with those from wind-tunnel tests for the same wing.

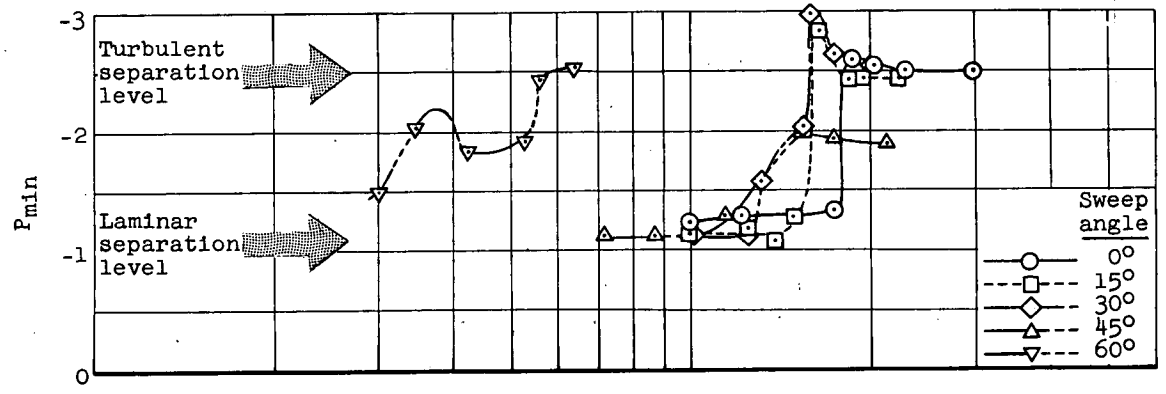

(a) Variation of minimum pressure coefficient with Reynolds number for a swept circular cylinder, reference 12.

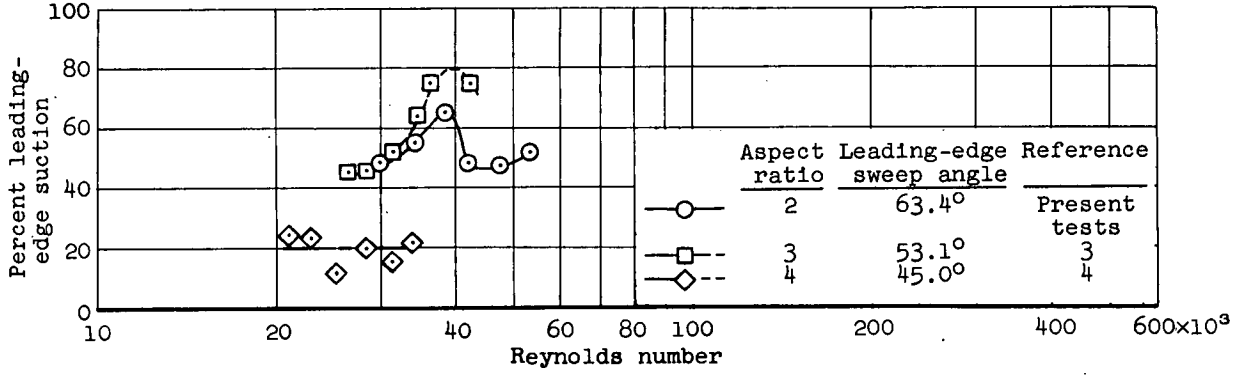

(b) Variation of leading-edge suction with Reynolds number for a family of triangular wing, exposed wing panels.

Figure 18.- Comparison of effect of Reynolds number on leading-edge suction of triangular wings and on minimum-pressure coefficients of swept circular cylinders; Reynolds number is based on wing leading-edge radius or cylinder radius and velocity perpendicular to leading edge or cylinder axis.

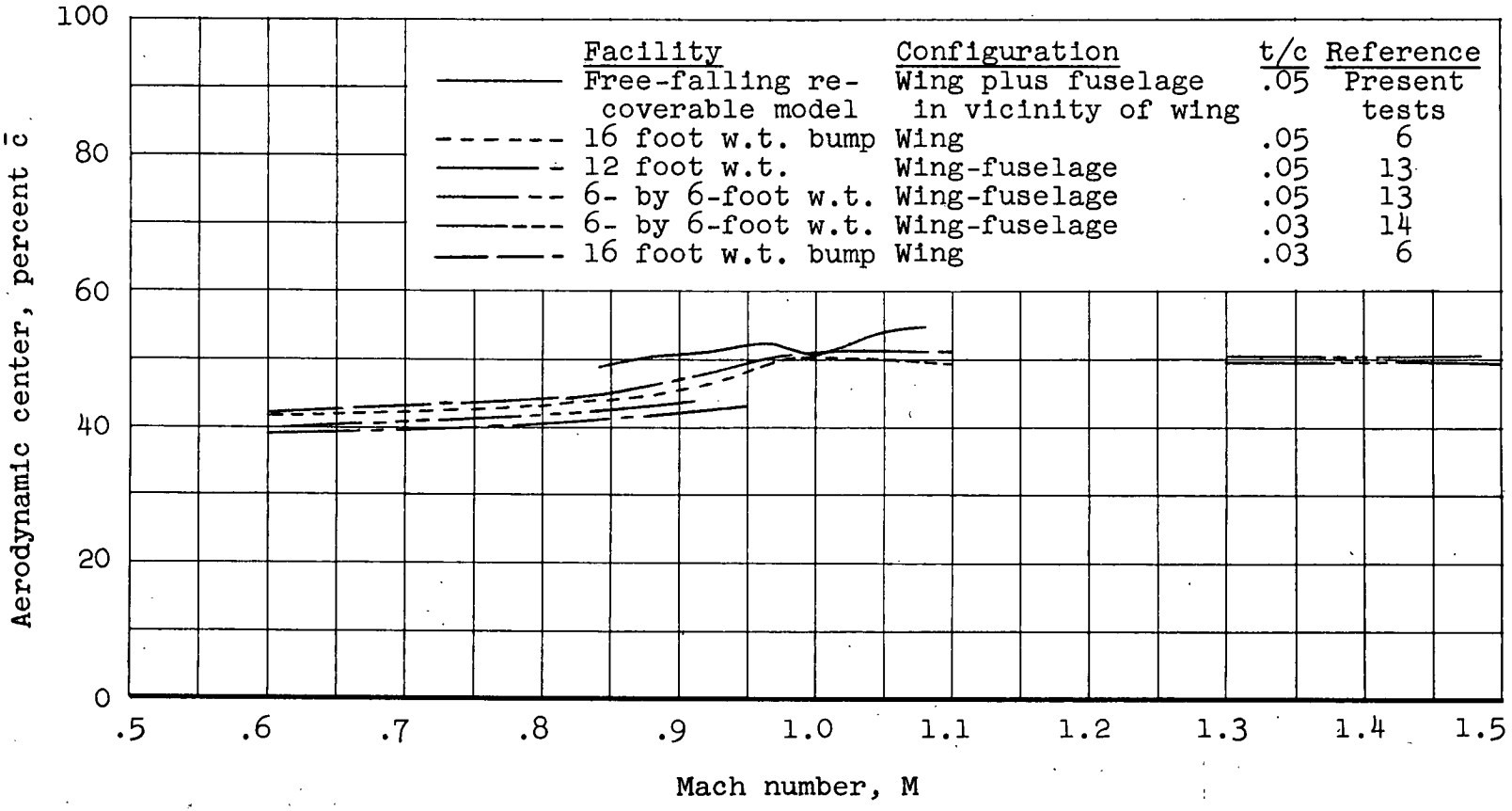

Figure 19.- Comparison of aerodynamic-center movements of the complete wing with those measured in wind-tunnel tests for low lift coefficients.

PERSONAL PROPERTY
OF J. R. CLARK